Marine Mammal Science

ARTICLE OPEN ACCESS

Comparing Drone and Vessel-Based Imaging to Quantify Epibiont Coverage on Humpback Whales

Isabel A. R. Taylor[1] | Ticiana Fettermann[2] | Barry McGovern[2] | David S. Schoeman[1,3] | Adrian B. McCallum[1] | Stephanie H. Stack[4,5]

[1]University of the Sunshine Coast, School of Science, Technology and Engineering, Sippy Downs, Queensland, Australia | [2]Pacific Whale Foundation Australia, Urangan, Queensland, Australia | [3]Centre for African Conservation Ecology, Nelson Mandela University, Gqeberha, South Africa | [4]Southern Ocean Persistent Organic Pollutants Program, School of Environment and Science, Griffith University, Nathan, Queensland, Australia | [5]Pacific Whale Foundation, Wailuku, Hawaii, USA

Correspondence: Stephanie H. Stack (stephanie.stack@griffithuni.edu.au)

Received: 12 July 2025 | **Revised:** 12 July 2026 | **Accepted:** 1 August 2026

Keywords: aerial imagery | color thresholding | commensal | ectoparasite | epizoite | health assessments | Mysticeti | proportional coverage | skin health

ABSTRACT

Cetacean epibionts offer noninvasive insights into host health, physiology, and spatial ecology, yet quantitative assessments in wild populations remain scarce. Although vessel-based observations may be limited by field of view and analyst input, unoccupied aerial vehicles (UAVs; drones) are increasingly used to monitor cetacean health indices, enhancing observational availability and reproducibility. However, the suitability of drones for quantifying epibiota has not been thoroughly evaluated. Implementing a standardized workflow, we compared dorsal proportional epibiont coverage estimates derived from drone-based imagery and traditional vessel-based techniques across reproductive classes of humpback whales (*Megaptera novaeangliae*). We analyzed 32 paired datasets using pixel-based methods, incorporating semiautomated graph-cut segmentation and iterative color-thresholding. Drone-derived estimates of epibiont coverage consistently exceeded vessel-based measures, which averaged 58% of the relative coverage estimated from corresponding drone imagery, partly attributable to variable lighting during image capture. Nevertheless, 94% of paired observations differed by less than 5% in absolute coverage, indicating strong agreement. While refinement of flight parameters, image resolution, and further validation are recommended, we demonstrate that drones can provide a reliable source of quantitative epibiont data, with potential applicability across diverse epibiont–host systems, benefiting cetacean population health monitoring programs and informing conservation strategies, particularly for elusive or understudied species.

1 | Introduction

Effective monitoring of aquatic wildlife and their interactions with the environment is crucial for understanding ecosystem health and guiding conservation efforts (Wikelski and Cooke 2006). In recent years, the use of unoccupied aerial vehicles (UAVs), or "drones," has significantly advanced the study of marine megafauna biology, including morphometrics (Dawson et al. 2017; Durban et al. 2016; Ejrnæs and Sprogis 2021; Glarou et al. 2023; Johnston et al. 2022), spatial organization and abundance (Angliss et al. 2018; Goebel et al. 2015; Sykora-Bodie et al. 2017), microbial and molecular analysis (Atkinson et al. 2021; O'Mahony et al. 2024; Pirotta et al. 2017), including photographic identification of individuals (Koski et al. 2015; Landeo-Yauri et al. 2020; Ryan et al. 2022). Drones have emerged as relatively cost-effective, scalable tools for marine mammal sampling (Álvarez-González et al. 2023; Sorrell et al. 2019), enhancing observational capacity and enabling physiological data collection at localized spatial scales (Costa et al. 2022; Hodgson et al. 2020; O'Callaghan et al. 2024; Torres et al. 2018).

The vertical perspective provided by drone imagery has facilitated precise photogrammetric measurements of cetaceans, including large whales (Dawson et al. 2017; Dickson et al. 2021; Durban et al. 2016; Johnston et al. 2022) and delphinids (Cheney et al. 2022; Christie et al. 2022; Currie et al. 2021; Vivier et al. 2023). These measurements are obtained by measuring pixel dimensions in drone images and converting them to real-world units using the camera's focal length and flight altitude, typically recorded via a laser rangefinder or pressure altimeter (Álvarez-González et al. 2023). Such measurements enable the estimation of dorsal surface area, body mass, or volume (Aoki et al. 2021; Glarou et al. 2023; Soledade Lemos et al. 2020). These derived biometrics are frequently used to evaluate body condition (e.g., Christiansen, Sprogis, et al. 2020; Christiansen et al. 2018; Napoli et al. 2024; Serres et al. 2024), a physiological index reflecting an individual's energy reserves, serving as a proxy for fitness and survivorship (Castrillon and Bengtson Nash 2020; Millar and Hickling 1990; Peig and Green 2010).

While the use of drones to study vulnerable cetaceans may be less intrusive than traditional vessel-based approaches (Christiansen et al. 2016; Christiansen, Nielsen, et al. 2020; Sprogis et al. 2023), their operation is limited by battery longevity and environmental conditions (Joyce et al. 2019; Raoult et al. 2020). The use of drones in marine mammal research is often constrained by precipitation and high wind speed (i.e., > 20 km/h) (Dickens et al. 2021; Raoult et al. 2020), with data quality further being impacted by sun angle, animal body angle, and tidal state (Christiansen et al. 2018; Hodgson et al. 2013). Nevertheless, when acquired under satisfactory conditions, drone imagery has proven highly effective for collecting high-quality data on cetacean ontogeny and behavior, often outperforming conventional vessel-based methods (e.g., Fettermann et al. 2022; Jones et al. 2022; Ryan et al. 2022; Sprogis and Christiansen 2024; Torres et al. 2018). However, the relative performance of drone-based versus traditional imaging approaches across taxa and research contexts remains insufficiently tested, highlighting the need for comparative studies to validate and refine the use of drones as a reliable data-collection tool (Garcia-Garin et al. 2020; Wirsing et al. 2022). Notably, few studies have directly compared drone- and vessel-based imaging approaches to quantify cetacean external anomalies, such as epidermal disease or anthropogenic scarring from vessel strikes and entanglements (Keeling et al. 2025; Leslie et al. 2022; Ramp et al. 2021). A common conclusion across these studies is that multiplatform approaches are most effective when they involve concurrent acquisition of comparable imagery from the same individual whales, allowing for robust comparisons and the identification of the most suitable observational tools for specific research objectives. However, such comparative studies remain rare, particularly for drone-based imaging approaches in wildlife research, where validated noninvasive methods are needed.

One promising use of drones involves the study of cetacean epibionts, organisms living on the exterior of cetacean hosts, either commensally or parasitically (Correia et al. 2023). Cetaceans support diverse epibiotic communities ranging from algae to fish, affecting the host integument to varying extents (Geraci and Aubin 1987). Their suitability as biological indicators in cetaceans includes providing insights into host health (Aznar et al. 2010, 2005; Osmond and Kaufman 1998; Stack et al. 2024), habitat use and migration routes (Taylor et al. 2019; Visser et al. 2020), stock differentiation (Urian et al. 2019), abundance shifts (Ten et al. 2026), and population structure and phylogeography (Bradford et al. 2011; Bushuev 1990; Kaliszewska et al. 2005). Commensal epibiont settlement has been suggested to reflect host hydrodynamics and oceanographic conditions, including water temperature and salinity (Aguilar and Raga 1993; Briggs and Morejohn 1972; Carrillo et al. 2015; Dolezal et al. 2023; Fish and Battle 1995; Kasuya and Rice 1970; Moreno-Colom et al. 2020; Ten et al. 2025). Despite their value as noninvasive indicator tools of marine ecosystems and host health, systematic quantitative studies of epibiota on live cetaceans remain scarce (Geraci and Lounsbury 2005; Minton et al. 2022; Ten, Raga, and Aznar 2022).

Reports on cetacean epibionts often rely on observations from stranded or deceased animals (e.g., Aguilar and Raga 1993; Groch et al. 2018; Iwasa-Arai et al. 2021; Kim et al. 2020; Qiao et al. 2020). While systematic studies have quantitatively examined epibiont diversity, density, and attachment locations across various cetacean species (Carrillo et al. 2015; Ólafsdóttir and Shinn 2013; Ten et al. 2025; Ten, Konishi, et al. 2022), these methods are limited by accessibility and their application to wild populations (Correia et al. 2023). Vessel-based imaging techniques have been employed to document the prevalence of epibiota in free-swimming cetaceans (Dolezal et al. 2023; Hanninger et al. 2023; Matthews et al. 2020; Whitehead et al. 2015). However, these health assessment studies may be subject to biases owing to the use of semi-quantitative evaluations (i.e., scoring systems) (Boileau et al. 2024; Pettis et al. 2004) or images acquired solely for identification purposes (Bradford et al. 2012; Minton et al. 2022; Towers et al. 2013; Urian et al. 2019). Although vessel platforms provide detailed lateral views, they are constrained by a limited field of view, likely underestimating epibiont abundance and distribution (Correia et al. 2023; Hunt et al. 2013; Vilches et al. 2023). Drones present a potential solution by providing broader, more consistent top-down perspectives of focal individuals. Though their effectiveness in documenting the impacts of ectoparasites has been demonstrated (Herr et al. 2023), coverage-based quantification, particularly across individuals of varying body size, has been proposed but not yet empirically tested (Moore et al. 2021; Ten, Konishi, et al. 2022).

Humpback whales (*Megaptera novaeangliae*) host particularly diverse epibiont communities (Fertl and Newman 2018; Ten, Raga, and Aznar 2022), possibly due to their extreme migratory life histories (Bortolotto et al. 2021; Horton et al. 2020). In the Southern Hemisphere, the International Whaling Commission (IWC) recognizes seven Breeding Stocks of humpback whales, labeled A through G (Clapham et al. 2009; Hauser et al. 2010). Each stock transitions between high-latitude summer feeding grounds and low-latitude winter breeding and calving grounds (Chittleborough 1965; Clapham and Mead 1999; Dawbin 1966). These populations faced near extinction in the late twentieth century following a century-long overexploitation (Clapham et al. 1999). Since then, humpback whales that migrate along the eastern coastline of Australia (IWC-designated Breeding Stock E1) have shown a marked recovery (Bejder et al. 2016; Noad et al. 2019). However, this population currently faces multiple conservation threats, including ship strikes, entanglement in fishing gear, pollutants, ocean noise, tourism pressure, and both the direct and compounding effects of climate change (Das et al. 2017; International Whaling Commission 2020; Mayaud et al. 2022; Minton et al. 2022; Pallin et al. 2023; Rossi-Santos 2015; Stack et al. 2021; Thomas et al. 2016; von Hammerstein et al. 2022). Integrating epibiont data into health monitoring programs can yield valuable insight into cumulative stressors and inform conservation strategies (Correia et al. 2023; Hermosilla et al. 2015; Herr et al. 2020; Pettis et al. 2004; Ten, Raga, and Aznar 2022).

This study examines the effectiveness of drone imagery relative to traditional vessel-based techniques for estimating epibiont loading on Breeding Stock E1 humpback whales during their southward migration from breeding and nursing grounds of the southern Great Barrier Reef (GBR) to Antarctic feeding grounds (IWC Antarctic Management Areas IV, V, and VI; Andrews-Goff et al. 2018; Smith et al. 2012). Using a paired, pixel-based quantitative approach with concurrently captured drone- and vessel-based images, this study aims to: (i) compare the precision of these two imaging platforms in quantifying epibiont coverage on standardized dorsal-surface anatomy of humpback whales, and (ii) evaluate specific methodological, environmental (e.g., lighting conditions), and biological (e.g., body orientation, surfacing behavior) covariates that may influence both detection accuracy and observational capacity. As a model system, we focus on colonized coronulid, or acorn barnacles (*Coronula diadema* and *C. reginae*), which are host-specific to humpback whales and can grow up to 5.5 cm in diameter and 3 cm in height, often providing substrate for clusters of gooseneck barnacles (e.g., *Conchoderma auritum*), reaching total lengths of 8 cm (Clarke 1966; Kim et al. 2020). Prior barnacle attachment scars are typically characterized by circular (mature) or star-shaped (juvenile) markings that appear as black-on-white and white-on-black skin (Bradford et al. 2011). These semipermanent features have been included in visual health assessments and individual photo-identification studies of humpback whales (Franklin et al. 2020; Minton et al. 2022). Coronulid barnacles and their associated scars are both prevalent in the E1 population and visually distinct, making them ideal biological markers for evaluating image-based detection. Through pairwise comparison, we assessed whether drone imagery can serve as a reliable substitute for, or complement to, vessel-based imaging techniques. Specifically, we aimed to evaluate the comparative efficacy of these approaches for monitoring epibiont prevalence and abundance in wild cetacean populations.

2 | Methods

2.1 | Study Population and Sampling Locations

Fieldwork was conducted at two locations along the eastern coastline of Australia: Hervey Bay, Queensland, and Eden, New South Wales (Figure 1). Hervey Bay is a hypersaline embayment (Ribbe 2014) centered at 25° S, 152.84° E, just south of the Great Barrier Reef Marine Park (GBRMP) and is within the Great Sandy Marine Park (GSMP). The mouth of Hervey Bay is ~80 km wide, opening to the north and narrowing southward, with a mean depth of ~20 m and a total area of ~4000 km^2 (Ribbe 2014). The area is an important early stopover site during the southern migration for up to one-third of the breeding stock of the E1 population of humpback whales (Chaloupka and Osmond 1999). It provides crucial habitat for socializing and resting, particularly for females and mother–calf pairs (Franklin et al. 2018, 2021; McGovern et al. 2025; Stack et al. 2019). Published estimates indicate a peak abundance of 2546 whales (95% CI: 1956–3135) and a linear increase of 118 whales per year (Brooks et al. 2024). Hervey Bay has been the focus of our extensive photo-identification research efforts since 1984 (Kaufman et al. 2011, 1987; Stack et al. 2019), with drone-based sampling initiated in 2021.

The waters off Eden, New South Wales (37.07° S, 149.90° E), comprise a relatively shallow coastal region (mean depth: ~61 m; Stamation et al. 2007) that lies along a narrow migratory corridor used by the E1 population of humpback whales before they return through deeper offshore waters to the Southern Ocean via Tasmania or New Zealand (Burns et al. 2014; Johnson et al. 2022). The region is known for large aggregations of migrating humpback whales, and opportunistic feeding behavior has also been documented (Pirotta et al. 2021; Stamation et al. 2007).

We collected paired drone-derived morphometric measurements and vessel-based photographic images of individual humpback whales in 2022 and 2023. Fieldwork was conducted primarily in Hervey Bay, Queensland, between July and October prior to southward migration. In October 2023, we also collected paired imagery over 5 days off Eden, New South Wales, concurrently with a separate body condition study. These data were collected to expand spatial coverage and assess the potential for resampling individuals across locations. Although no individuals were matched between Hervey Bay and Eden, the paired drone and photographic data collected in Eden met the inclusion criteria for the present analysis, as described in Sections 2.3.1 and 2.3.2 below, and were therefore included to broaden geographic representation.

Data collection in Hervey Bay, QLD, was authorized under a Marine Parks Research Permit P-MPR-100853077, Scientific Purposes Permit P-SPP-100853084, and approval from the Animal Ethics Committee of the Queensland Government. Data collection in Eden, NSW, was authorized under a DCCEEW Cetacean Permit 2023–0007, Scientific License SL102792, and approval from the Animal Ethics Committee of Griffith University. All drone operators held a Civil Aviation Safety Authority (CASA) remote pilot license.

2.2 | Data Collection

Concurrent photographic and video data were collected within Hervey Bay, Queensland, and at Eden, New South Wales, using a 5.9-m rigid inflatable boat fitted with a 250 HP outboard motor, and a 6.4-m aluminum-hulled vessel with two 80 HP Yamaha motors, respectively. Surveys were conducted in daylight under calm, clear, and dry conditions (i.e., no rain or fog), with Beaufort sea states ≤ 3 and wind speeds < 10 knots. Humpback whales were detected opportunistically by sight and slowly approached to approximately 50 m for photo-identification and drone deployment. An onboard barometric altimeter was utilized in the field to maintain a minimum

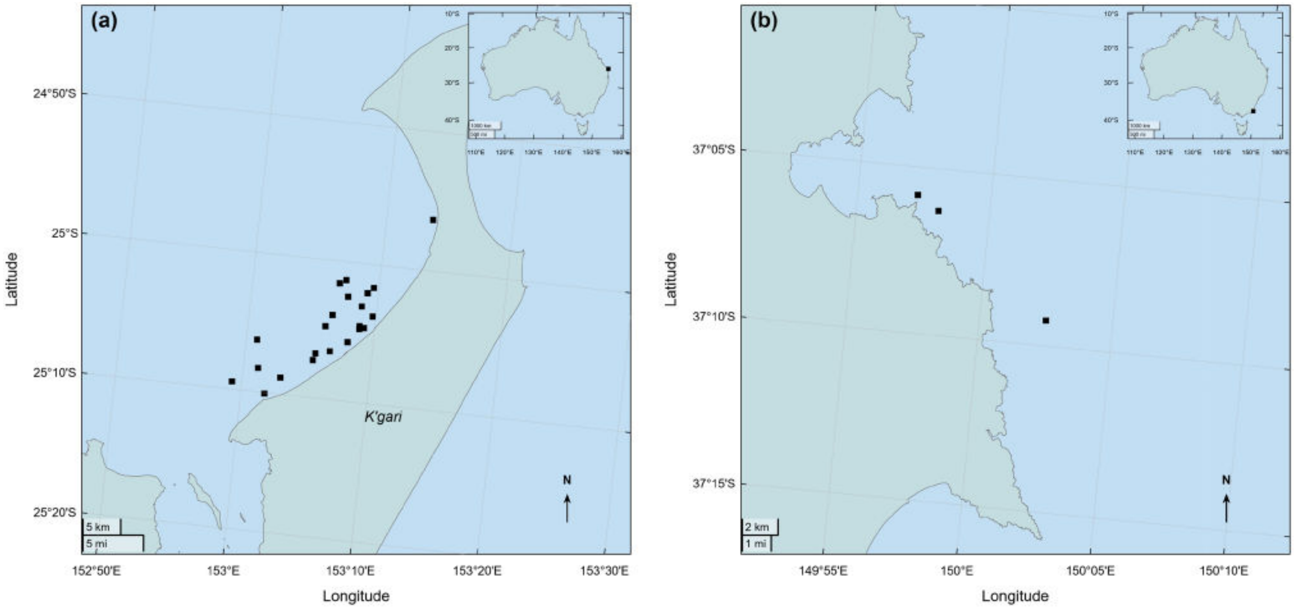

FIGURE 1 | Geographical context of concurrent vessel and drone imagery data collected from breeding stock E1 humpback whales (*Megaptera novaeangliae*) along Australia's eastern coastline at (a) Hervey Bay, Queensland, from July to October in both 2022 and 2023, and (b) Eden, New South Wales, over 5 days in October 2023. Black points denote the GPS locations of each paired-image sample.

flight altitude of 30 m, or up to 40 m when monitoring multiple mother–calf pairs. For every image attempt, we also documented the date, time, GPS location, sea state, and group composition. We assigned each recorded whale an age class based on field observations of body length and behavior, together with available photo-identification history from a long-term catalogue (Stack et al. 2019). All calves observed were older than neonates, following the description of neonatal calf characteristics provided by Cartwright and Sullivan (2009).

2.2.1 | Vessel-Based Image Acquisition

Multiple (2–3) Canon 6D Mark II DSLR cameras fitted with Canon 100–400 mm f/4.5–5.6 telephoto lenses were used to obtain identification images from the vessel. DSLR images were acquired with a shutter speed of 1/1500 s and ISO set to automatic. During vessel-based sampling, we targeted specific anatomical features, including near-perpendicular angles of the dorsal surface of the tail flukes and pectoral fin, as well as dorsolateral, or aerial-like angles of the rostrum (Figure 2). The rostral area was defined as the dorsal cranial area forward of the eyes, encompassed by the blowholes, upper jaw, and lip margins. This area was selected to avoid underestimating the lateral mandibular jaw, which is often obscured in vertical view. These anatomical regions were standardized based on their consistent visibility in both drone and vessel-based imagery and are also where the colonization of sessile barnacles is commonly observed in this species, particularly around the tubercles of the rostrum and pectoral fin leading edge (Shea and Gallagher 2021). The dorsum was excluded from quantitative analysis due to difficulties in standardizing surface area estimates from variable lateral images of the flank (Minton et al. 2022) and to avoid underestimating this curved region relative to the more consistent top-down perspective provided by drone imagery.

2.2.2 | Drone-Based Image Acquisition

During encounters with humpback whales, a DJI Inspire 2 Pro quadcopter equipped with a Zenmuse X5S gimbal camera and an Olympus 25 mm f/1.8 lens (sensor size: 17.3 × 13.0 mm) was flown to capture high-resolution video used in body condition assessments. Camera exposure settings, including shutter speed and ISO, were controlled automatically by the drone camera and were not standardized across flights. Drone videos were recorded at a resolution of 4 K and 30 frames per second (pixel dimensions: 0.0045 mm/pixel). The drone was launched and recovered manually from the vessel and fitted with a custom-mounted SF11/C (120 m) laser altimeter (*LightWare LiDAR*, South Africa) to obtain precise height measurements. All aerial data were collected with the gimbal pitch set to nadir (90°) to ensure that focal animals were centered within the field of view and to minimize perspective distortion associated with oblique imagery (Burnett et al. 2019; Joyce et al. 2019; Segre 2025). Ground Sampling Distance (GSD) is a standard metric for evaluating image resolution at ground level (e.g., mean sea surface level), defined as the real-world distance represented by a single pixel (Torres and Bierlich 2020). Based on the specifications of the drone camera and the flight altitude, GSD was computed individually for all utilized drone stills to evaluate its potential effect on proportional coverage estimates (see Section S.1).

2.3 | Image Selection Criteria

2.3.1 | Vessel-Based Data

All available vessel-based images taken during both survey seasons were manually scanned to identify the presence and/or prior attachment of epibionts on the dorsal surface of target anatomies. Individuals with as few as one attached commensal barnacle were

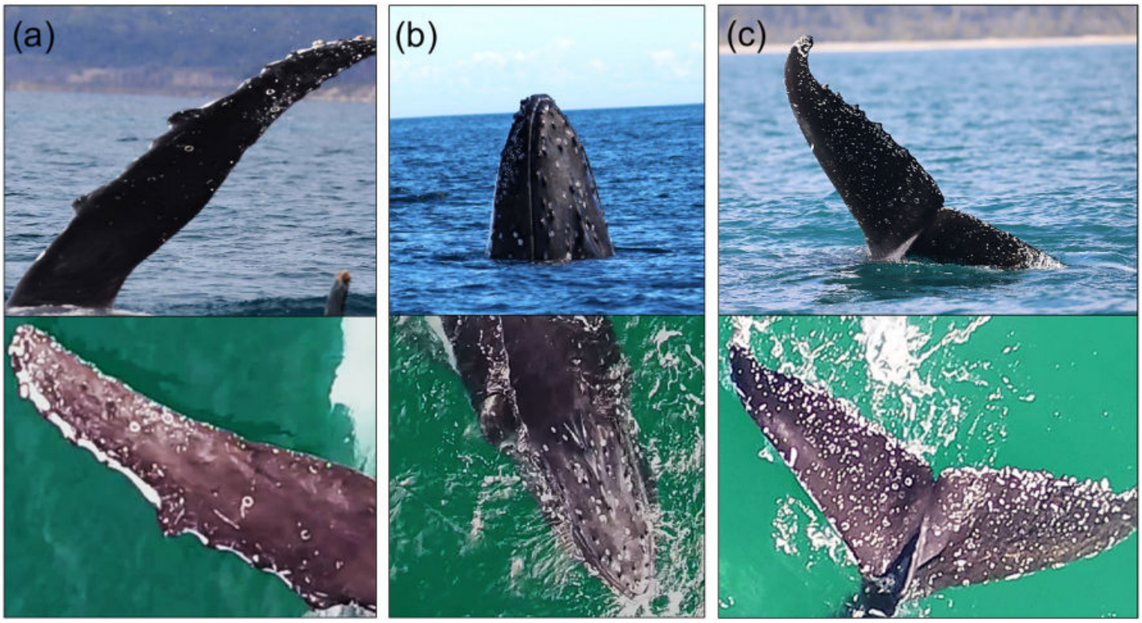

FIGURE 2 | Examples of vessel- and drone-based imagery utilized in a pairwise comparison for estimating epibiont barnacle scar coverage on the dorsal surface of humpback whales (*Megaptera novaeangliae*). The images in the panels show paired data captured from the same individual animal for (a) the pectoral fin, (b) the rostrum, and (c) the right fluke blade. The upper images in the panels are derived from vessel-based DSLR cameras, and the lower images are the corresponding drone video stills.

included in the pairwise dataset. Epizoites located along appendage trailing edges that extended beyond the defined anatomical surface areas (e.g., *C. auritum*) were excluded from this analysis. Vessel-based images containing evidence of epibiont-affected areas of humpback whale skin were subjected to an adapted quality grading based on the methods by Calambokidis et al. (2008). This included five criteria: (i) visibility of the relevant anatomy, (ii) angle of the anatomy relative to the water surface, (iii) angle and orientation of the animal from the photographer at the time of image capture, (iv) glare (exposure/contrast), and (v) focus (sharpness). Each criterion was rated from 1 to 5, with 5 indicating top quality, and any image that scored less than 3 on any criterion was excluded. The cumulative quality grade for each unedited image was determined as follows: 5 (*excellent image with the target anatomy positioned at a perpendicular-to-the-observer angle*), 4 (*good*), 3 (*average*), 2 (*fair*), and 1 (*poor*). Following Ten, Konishi, et al. (2022), qualitative evaluations of dorsal surface epibiont abundance (e.g., attached *Coronula* spp.) in quality-graded vessel-based images were used to establish an Intensity Estimate (IE) baseline. The images were assigned scores based on the visual count of individual epibionts within each image: “1” for 1–20 coronulids, “2” for 21–100 coronulids, and “3” for over 100 coronulids, reflecting low, moderate, and high coverage, respectively (Figure 3).

2.3.2 | Aerial Imagery

Corresponding drone video footage of photographed whales that passed quality grading and showed evidence of epibionts and/or prior attachment scars within the predefined anatomical landmarks was manually examined using VLC Media Player (https://www.videolan.org/vlc/). Multiple frames (‘stills’) were extracted from videos of the same encounter for consideration, where the focal animal's anatomical landmark was positioned at or above the surface. Drone imagery met strict environmental and image-quality criteria, including clear focus, absence of distinguishable glare spots, particularly around rostral area tubercles (Evans et al. 2026), animal pitch (vertical plane positioning of the target anatomy), and sea-surface conditions (no water disturbance, spray, or ripples), following guidelines similar to Christiansen et al. (2018). Based on these criteria, quality grades were assigned as “3” (*good*), “2” (*average*), or “1” (poor). Aerial video stills assigned a quality grade 1 for any criterion were excluded (Figure S1). When multiple suitable stills were available from the same encounter or individual, the best-quality frame was selected. Image selection prioritized the visibility and orientation of focal anatomical landmarks, which differs from traditional approaches that emphasize full-body posture in body condition assessments.

2.4 | Image Processing

All quality-filtered images of standardized anatomical regions acquired from drone and DSLR platforms were digitally analyzed using a semiautomated workflow to estimate proportional epibiont coverage for each image-capture technique. Image processing was conducted in MATLAB Version R2023b (The MathWorks Inc., Natick, MA, USA) using the *Image Processing Toolbox* functions (https://www.mathworks.com/products/image-processing.html). The *Image Processing Toolbox* enabled a pixel-based proportion analysis similar to the approach used by Leslie et al. (2022) and was applied to both vessel- and drone-based image data. By selecting comparable anatomical landmarks (Figure 4), we maintained relative consistency between drone- and vessel-based imagery, enabling direct quantitative comparison of the two sampling techniques. Images were not adjusted for shadows, brightness, contrast, or other visual properties prior to analysis, thereby avoiding potential masking or enhancement of pixels relevant to epibiont detection.

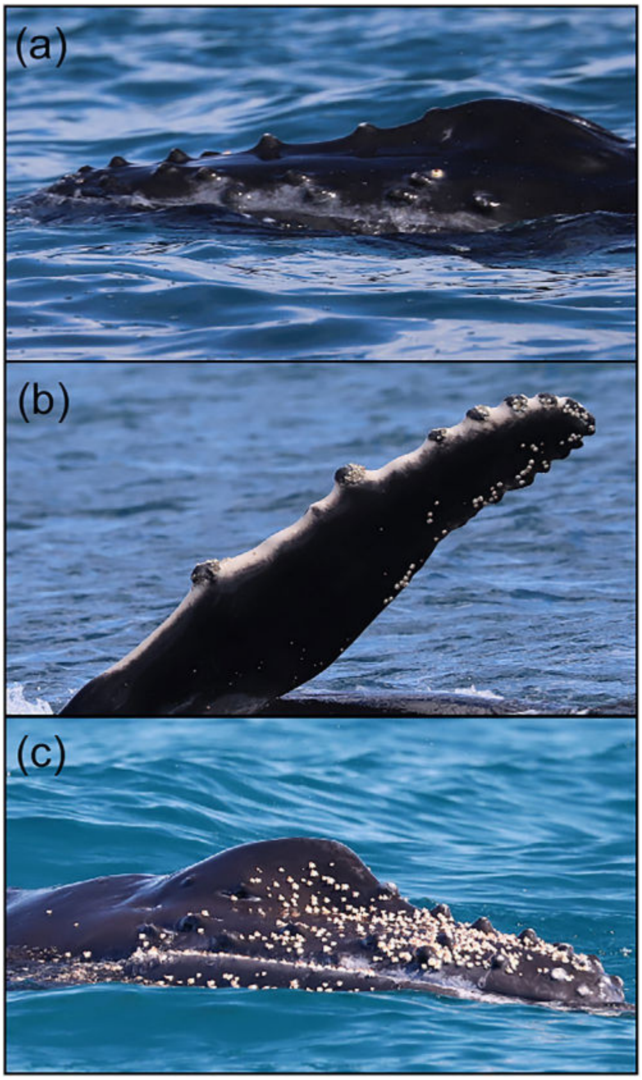

FIGURE 3 | Examples of vessel-based images of standardized dorsal-surface regions used to assign intensity estimate (IE) scores for attached *Coronula* spp. on the rostrum and pectoral fins of humpback whale (*Megaptera novaeangliae*) calves. Images are selected based on comparability with corresponding drone video footage captured concurrently. The examples shown are from three calves photographed in Hervey Bay, Queensland. Manual evaluation of coronulid barnacle abundance in each image corresponds to: (a) low coverage (1–20 barnacles; IE = 1), (b) moderate coverage (21–100 barnacles; IE = 2), and (c) high coverage (> 100 barnacles; IE = 3).

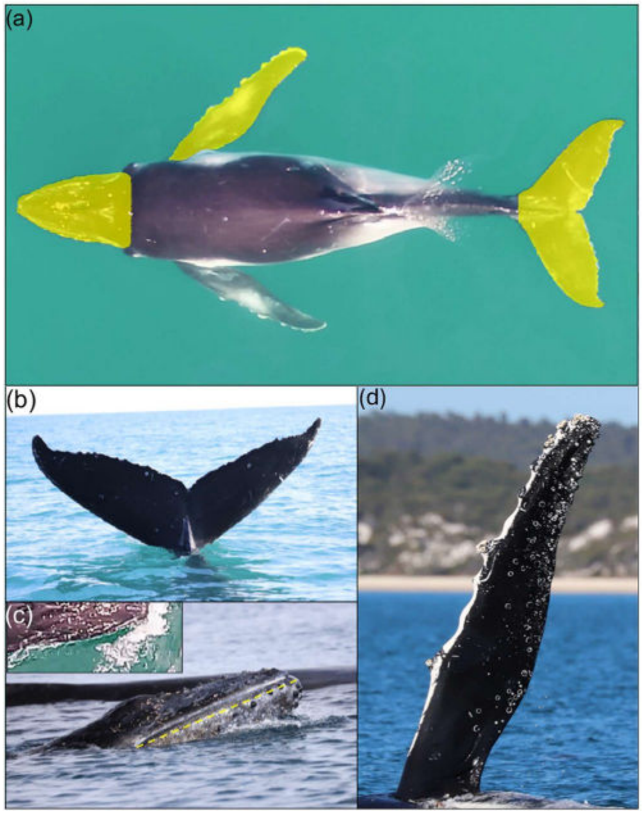

FIGURE 4 | Aerial and vessel-based perspectives of humpback whales (*Megaptera novaeangliae*) illustrating the standardized anatomical regions used for image analysis. (a) Yellow-masked areas indicate the three dorsal-surface regions targeted in the comparative analysis: The rostral area, pectoral fin, and tail flukes. (b) Vessel-based image of the dorsal surface of the flukes showing barnacle scars and exemplifying a near-perpendicular angle (image quality score = 4) suitable for pairwise comparison with top-down drone imagery. (c) Lateral vessel-based image of the rostrum with attached juvenile *Coronula* spp.; the yellow dashed line indicates the ventral boundary of the analyzed region, matched to the corresponding side of the rostrum in the drone image. (d) Vessel-based image of the dorsal surface of the pectoral fin, also captured at a near-perpendicular angle (image quality score = 4).

To maximize sample size, vessel-based images capturing either the left or right side of the rostrum were included. The use of single-sided images was accounted for in paired analyses by restricting measurements in the corresponding drone video stills to the same rostral half (Figure 4c), delineated using tubercles and lip margins as anatomical boundaries. Similarly, vessel-based images capturing a single fluke blade (delineated by the fluke notch) or dorsal-side flukes photographed during a dive sequence (i.e., at approximately a 45° angle) were included. In these cases, the corresponding visible area was delineated within the paired drone imagery to ensure consistency in surface area measurements. Drone stills were manually cropped to reduce visual interference, such as non-targeted whales or other whale anatomy not relevant to the study. These stills were analyzed prior to corresponding vessel-based images to reduce observer bias by minimizing potential influence from the higher resolution of the vessel-based imagery. To evaluate segmentation variance, defined as the variability in repeated pixel-based estimates of epibiont coverage from the same image, we randomly selected six whales from the paired-image dataset. For each whale and each targeted anatomical region (rostrum, pectoral fin, or tail fluke), we analyzed the corresponding paired drone and vessel-based images, all of which had passed initial quality filtering. Each image was measured five times, resulting in a total of 60 replicate measurements (Table S1.1).

2.4.1 | Graph-Cut Segmentation

Digital image analysis began with semiautomated segmentation of red, green, blue (RGB) images to separate the anatomical region of interest (ROI) from the surrounding background. We applied the interactive Graph Cut tool in MATLAB's

Image Segmenter application to all input images. Graph-cut segmentation treats each pixel as a node in a graph and separates foreground and background by minimizing an energy function known as the "cut," which defines the optimal boundary between regions (Rother et al. 2004). Foreground pixels are connected to a source node (s-node) and labeled "1," while background pixels are connected to a sink node (t-node) and labeled "0." In the present study, this approach effectively separated high-contrast foreground features from complex backgrounds, including images captured close to land. The interactive Graph Cut tool enabled efficient user selection of foreground and background regions to generate black-and-white (BW) binary image masks (BIMs), which were used to extract pixel abundance from the segmented anatomical region of interest (ROI). We then applied the Active Contours function to refine the initial segmentation by automatically adjusting mask erosion and dilation, with additional manual refinements performed via the Paint Brush tool. This process produced segmented RGB image mosaics saved as .MAT files for further processing. Each paired image sample, labeled by its Sample ID, yielded two BIMs relating to the anatomical ROI: one derived from the drone still and one from the corresponding vessel-based image.

2.4.2 | Thresholding-Based Segmentation

Segmented RGB image mosaics, defined during the graph-cut step and representing anatomical ROIs, were further classified using color information to isolate pixels corresponding to attached epibionts or scars from prior attachments, distinguishing them from the surrounding humpback whale skin. This process involved manually marking masked RGB images using color space selection and color thresholding segmentation. The iterative evaluation of available color space variants in MATLAB's *Color Thresholder* application led to the selection of the $L^*a^*b^*$ color space for all images. Comprising three channels, L^* (luminance), a^* (high-red to low-green), and b^* (high-yellow to low-blue), this color space was optimal for detecting white circular scars on blue-black skin and yellow-orange-red hues of epibiotic fauna (Figure S2). Critically, the $L^*a^*b^*$ color space specifies color in absolute values, enhancing the accuracy and consistency of color-based analysis by accounting for human perception and variation in image display devices (Bora et al. 2015).

Threshold values for the color channels were established manually using the application's integrated histograms and point cloud plots to optimize secondary ROI extraction. The Polygon ROI tool transforms three-dimensional (3D) representations into two-dimensional (2D) arrays, enabling precise color segmentation by defining and adjusting polygons within the point cloud. Manual demarcation was favored over automatic thresholding due to its capacity to produce segmentation results with higher precision. A human-led examination of the ROIs was performed across all images to ensure exclusion of pixels associated with natural pigmentation or scarring unrelated to prior epibiont attachment. Secondary BIMs were generated for each image-acquisition source (drone- and vessel-based), with pixel classes labeled 0 and 1 and exported as .MAT files for computational analyses.

2.4.3 | Pixel-Based Analysis of Proportional Epibiont Coverage

Following the processing of the input images (Figure 5a), four BIMs (2D matrices) were generated for each sample (Sample ID), incorporating paired drone and vessel-based imagery. Each image-acquisition source produced two BIMs: an anatomical mask (DBIM1 or VBIM1) and an epibiont mask (DBIM2 or VBIM2). The first mask, containing pixels labeled as 1 following graph-cuts of the input images, was defined as the foreground or anatomical region in either the drone or vessel-based image (DBIM1 or VBIM1; Figure 5b). After applying color thresholding to the initial image mask, the barnacle- and barnacle scar-related pixels, labeled 1 in the secondary mask (DBIM2 or VBIM2; Figure 5c), were superimposed onto the original input images to visually verify segmentation accuracy (Figure 5d). The total number of class-1 pixels from the two image masks was extracted and subsequently used to calculate the relative proportionate coverage of whale skin affected by epibionts and related scars, where:

$$\text{Proportional coverage } (\%) = \left(\frac{\text{ROI pixels in epibiont BIM}}{\text{ROI pixels in anatomy BIM}}\right) * 100.$$

This formula yielded a pixel-derived estimate of proportional epibiont coverage within the standardized anatomical regions defined during the graph-cut segmentation step, enabling direct comparisons between aerial and vessel-based imaging techniques. Absolute differences were calculated as percentage-point differences between platform-specific proportional coverage estimates, whereas relative differences were calculated as the magnitude of this difference expressed proportionally. The image processing workflow used to quantify the percentage cover of epibiont-affected areas of whale skin, using the standardized dorsal anatomy, is illustrated by the schematic in Figure 6.

2.5 | Statistical Analyses

To analyze the vessel- and drone-based pairwise data, we applied Standardized Major Axis estimation (SMA, or Model II) regression. Unlike standard regressions, which predict one variable from another, SMA does not assume either dataset contains "true" values; instead, it only summarizes the relationship between the two variables when both have measurement error (Warton et al. 2012). A one-tailed t-test was additionally performed to assess the proportional relationship between vessel- and drone-based epibiont coverage estimates, with vessel-based estimates expressed relative to paired drone-based estimates. To further evaluate factors influencing proportional coverage estimates, we employed generalized linear mixed-effects models (GLMMs) with a beta error structure and a logit link function. Since the sample size was relatively small, models with complex interactions could not be reliably fit. To investigate potential methodological and biological effects on these estimates, we modeled proportional coverage as a function of the sampling platform, time of image capture (as a proxy for changing light conditions), GSD (cm/px), age class, anatomical region assessed, and epibiont characteristics (attached coronulid barnacles vs. barnacle scars). We also included the two-way interaction between the sampling platform and each of these predictors. Sample ID was included as a random intercept to account for

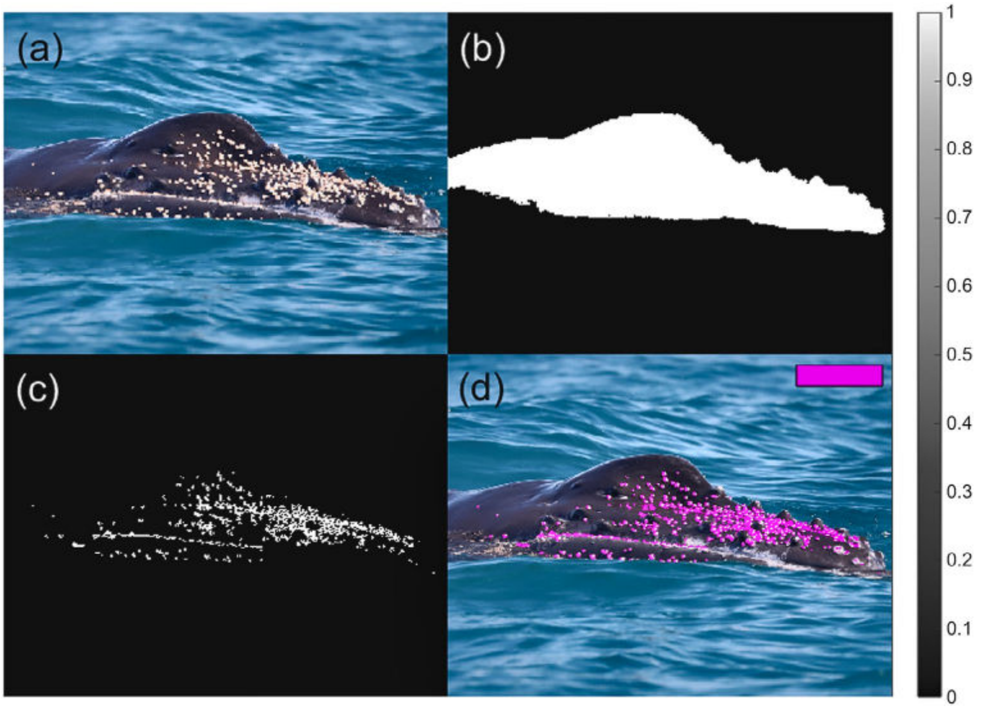

FIGURE 5 | Vessel-based quantification of the proportional coverage of colonized barnacle epibionts on the dorsolateral rostrum of a humpback whale calf. (a) Original input image. (b) Graph-cut segmentation separating the image foreground from its background counterparts, resulting in an initial binary image mask (VBIM1). (c) Secondary image mask created through color thresholding of the initial mask (VBIM2). (d) Original image overlaid with the pixel count (magenta) of the segmented area affected by epibionts. The scale bar indicates the binarized pixel values (0, 1) generated by each masked image in panels (b) and (c), respectively.

the non-independence of repeated measures (pseudo-replication). While cloud coverage can influence drone-based imaging over water (Joyce et al. 2019), average daily cloud cover (%) obtained from *Visual Crossing Weather Services* (https://www.visualcrossing.com/weather/weather-data-services) for each sampling location showed no observable effect during exploratory analysis and was therefore excluded from statistical models.

To assess factors influencing differences in BIM pixel counts, we used a GLMM with a Gaussian error structure and an identity link, treating Sample ID as a random effect. Image mask pixel count data were log-transformed prior to model fitting to approximate normality of residuals and homogeneity of variance. Model parsimony was evaluated using the corrected Akaike Information Criterion (AICc) for small sample sizes, accounting for the number of estimable parameters (K) (Anderson et al. 1994). Statistical significance was set at $\alpha = 0.05$, and covariates lacking substantial support were removed from the model. Final model assumptions were checked using standardized weighted residuals as a function of observation indices, and ANOVA tables were computed to evaluate the significance of covariates in the final models. To determine effect sizes, R^2 marginal (the proportion of variance accounted for by the fixed effects), R^2 conditional (the proportion of variance accounted for by both fixed and random effects), and intra-class correlation (ICC = intercept variance/(intercept variance + residual variance)) were computed. Additionally, Tukey *post hoc* tests for categorical effects were performed using estimated marginal means (EMMs) and 95% confidence intervals (CIs) to adjust for covariates and account for potential bias from confounding effects or imbalanced data (e.g., age class). All statistical analyses and graphical visualizations were conducted in R version 4.3.2 (R Core Team 2024) using the following packages: *lubridate* (Grolemund and Wickham 2011), *fitdistrplus* (Delignette-Muller and Dutang 2015), *glmmTMB* (Brooks et al. 2017), *emmeans* (Lenth 2024), *smatr* (Warton et al. 2012), *marginaleffects* (Arel-Bundock et al. 2024), and *MuMIn* (Bartoń 2024).

3 | Results

3.1 | Sample Composition Summary

Across the two study years, the filtration of imagery from 287 humpback whale encounters resulted in 32 paired estimates of proportional coverage, each derived from drone- and vessel-based imagery collected concurrently within the same encounter. The paired estimates represented 26 distinct encounters and 31 individual whales (Table 1). Two paired samples collected in Hervey Bay in 2023 originated from a single calf, with the right fluke blade and pectoral fin analyzed as separate anatomical samples. Within the vessel-based dataset suitable for direct comparison with drone imagery, adult whales were underrepresented ($n = 6$) relative to subadults ($n = 12$) and calves ($n = 14$). Drone imagery demonstrated greater observational capacity due to controlled camera angles, whereas corresponding vessel-based images were occasionally unavailable or did not meet the required quality and anatomical standardization criteria for pairwise comparison.

Of the 32 vessel-based image samples, 17 (53.1%) showed barnacle scars predominantly. These included dorsal-side flukes

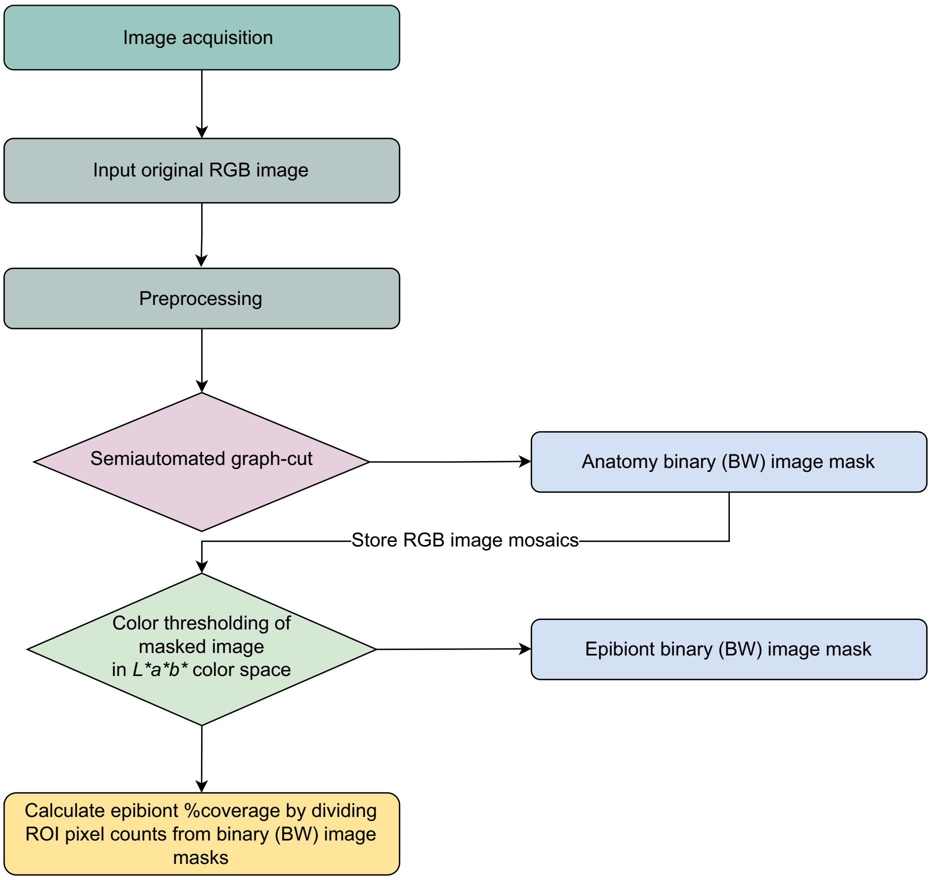

FIGURE 6 | Schematic of the image-processing workflow used in the RGB (red, green, blue) image-segmentation approach for estimating the relative proportional coverage of the standardized dorsal surface anatomy affected by epibionts.

($n = 11$), pectoral fins ($n = 5$), and one rostrum ($n = 1$) (Table 1). All subadult samples fell within this epibiont characteristic category, together with five adult samples. No evidence of prior barnacle attachment was observed on calf skin. The remaining 15 vessel-based image samples (46.9%) contained attached coronulid barnacles. Of these, calf rostral regions accounted for 12 samples (37.5%) and showed high (IE = 3, $n = 1$), moderate (IE = 2, $n = 8$), and low coverage (IE = 1, $n = 3$). The remaining moderate-coverage samples (IE = 2) were observed on dorsal-side tail flukes ($n = 2$; one adult and one calf) and on the pectoral fin of a calf ($n = 1$) (Table 1).

3.2 | Pairwise Comparisons

3.2.1 | Absolute Differences in Proportional Epibiont Coverage

Based on repeated measurements of six random paired samples, each measured five times ($n = 60$), manual marking during segmentation showed low variance across image platforms (Table S1.1). Standard deviations ranged from 0.07% to 0.45% for vessel-based images and 0.10%–0.83% for drone stills. Estimates of proportional epibiont coverage on the target anatomies varied from 0.34% to 10.93% in vessel-based images and from 1.11% to 16.45% in corresponding drone stills (Table 2). Drone-derived estimates were consistently higher than those derived from vessel-based images across all summary statistics and showed a broader range, with more extreme interquartile values (Q1–Q3) (Table 2 and Figure 7). In 75% of cases, vessel-based images of calf rostra showed fixed lateral views rather than perpendicular orientations relative to the observer. These samples required extra manual marking during the graph-cut segmentation process of the corresponding drone imagery to isolate either the left or right side of the rostrum. These one-sided samples showed lower absolute divergence between image-acquisition sources (median = 0.82%) than the dorsal-side fluke region (1.92%). Across anatomical regions, the smallest absolute difference between median platform estimates was observed for pectoral fins (0.79%).

3.2.2 | Sampling Platform Estimate Deviation

SMA (Model II regression) comparing drone- and vessel-based percentage coverage measurements revealed a strong, positive relationship between the two methods ($R^2 = 0.865$, $p < 0.001$; Figure 8), indicating that drone-based estimates increased disproportionately relative to vessel-based estimates. Further investigation into the proportional difference between the two techniques confirmed a statistically significant divergence between sampling estimates ($t(31) = -9.74$, $p < 0.001$, 95% CI [0.46, 0.71]; Table 3). Specifically, proportional coverage estimates derived from vessel-based imagery constituted approximately 58% of the relative coverage obtained from paired drone-based imagery.

TABLE 1 | Summary of barnacle epibiont coverage across age classes of eastern Australian humpback whales included in a comparative image-based analysis using paired drone- and DSLR-derived (vessel-based) samples ($N = 32$).

Age class	*n*	Vessel-based evaluation (scars/IE = 1–3)	Anatomical region	Area analyzed	Mean (±SD) vessel-based %coverage	Min vessel-based %coverage	Max vessel-based %coverage	Mean (±SD) drone-based %coverage	Min drone-based %coverage	Max drone-based %coverage
Calf	1	Low	Rostrum	Left side	—	0.34	0.34	—	1.11	1.11
Calf	1	Low	Rostrum	Right side	—	0.87	0.87	—	1.20	1.20
Calf	1	Low	Rostrum	Total	—	0.53	0.53	—	1.38	1.38
Calf	1	Moderate	Dorsal-side fluke	Right blade	—	0.6	0.6	—	2.62	2.62
Calf	1	Moderate	Pectoral fin	Total	—	1.1	1.10	—	2.06	2.06
Calf	3	Moderate	Rostrum	Left side	3.05 (±1.26)	1.59	3.78	3.82 (±1.90)	1.89	5.69
Calf	3	Moderate	Rostrum	Right side	2.21 (±1.05)	1.20	3.30	3.92 (±3.25)	1.86	7.66
Calf	2	Moderate	Rostrum	Total	1.75 (±0.49)	0.40	1.09	2.05 (±0.53)	1.67	2.42
Calf	1	High	Rostrum	Right side	—	10.93	10.93	—	16.45	16.45
Subadult	1	Scars	Dorsal-side fluke	Left blade	—	0.48	0.48	—	2.39	2.39
Subadult	1	Scars	Dorsal-side fluke	Right blade	—	2.83	2.83	—	8.22	8.22
Subadult	6	Scars	Dorsal-side fluke	Total	3.77 (±4.14)	0.6	10.52	5.91 (±4.25)	1.80	13.27
Subadult	3	Scars	Pectoral fin	Total	6.59 (±3.6)	4.1	10.71	8.20 (±5.03)	4.68	13.96
Subadult	1	Scars	Rostrum	Total	—	2.22	2.22	—	3.22	3.22
Adult	2	Scars	Pectoral fin	Total	3.41 (±3.01)	1.28	5.54	6.11 (±4.43)	2.98	9.25
Adult	1	Scars	Dorsal-side fluke	Left blade	—	5.98	5.98	—	10.80	10.80
Adult	2	Scars	Dorsal-side fluke	Total	2.70 (±0.11)	2.62	2.77	4.40 (±2.28)	2.79	6.01
Adult	1	Moderate	Dorsal-side fluke	Total	—	2.13	2.13	—	2.88	2.88

Note: Quantitative, pixel-based measurements of epibiont-affected areas were obtained from standardized dorsal anatomical regions in each image pair. Drone values were compared to corresponding vessel-based assessments of visible barnacle scars or attachment of coronulid barnacles. Intensity estimate (IE) scores were assigned via manual counts of attached coronulid barnacles observed on the rostrum, pectoral fin, or dorsal-side fluke (IE = 1: low coverage; IE = 2: moderate coverage; IE = 3: high coverage). The anatomical region analyzed is specified as total, left, or right side/blade, where applicable. For each age class, the number of paired samples (*n*), IE score, and anatomical region are listed alongside the mean, standard deviation (SD, in parentheses), and minimum/maximum absolute estimates of proportional epibiont coverage (%coverage), derived independently from drone and DSLR imagery.

TABLE 2 | Summary statistics for the absolute estimates of proportional epibiont coverage (%) derived from vessel- and drone-based images, including computed absolute differences using a pixel-based analysis.

Sampling platform	*N*	Min (%)	Q1 (%)	Median (%)	Q3 (%)	Max (%)
Vessel	32	0.34	1.04	2.13	3.86	10.93
Drone	32	1.11	2.20	3.10	6.73	16.45
Diff	32	0.09	0.72	1.29	2.87	5.52

Note: Reported values include the minimum, maximum, median, and interquartile range (Q1–Q3). Quantiles are presented here due to the right-skewed distribution relative to normality.

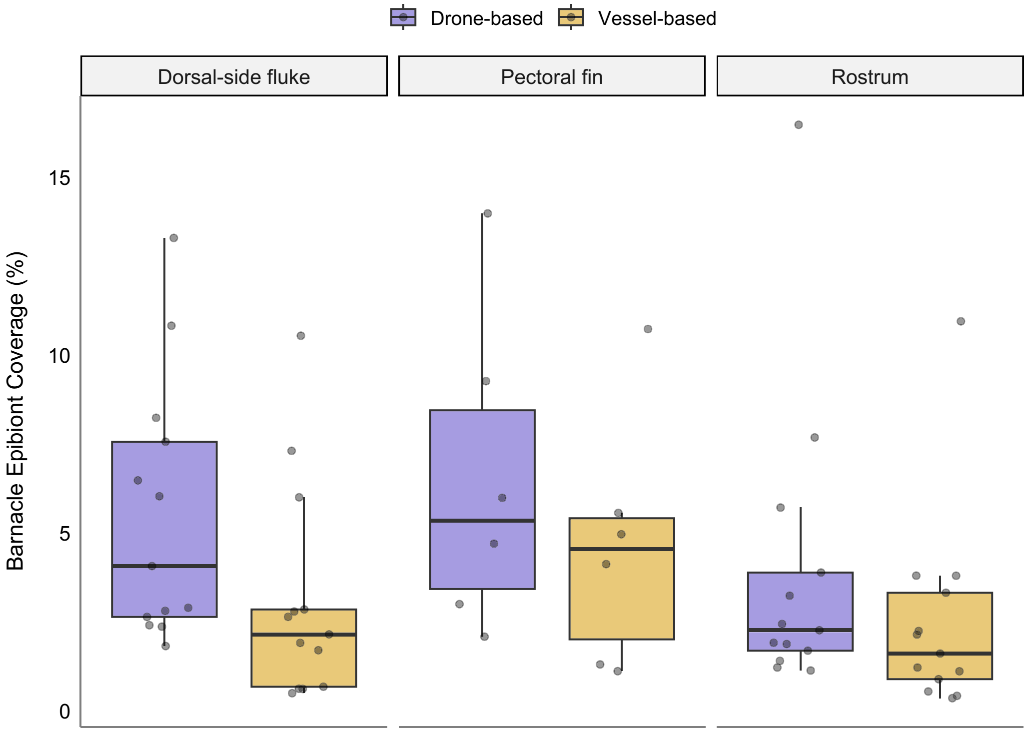

FIGURE 7 | Box plots show the distribution, median (bold horizontal lines), and spread of the paired image data (N = 32) for estimates of proportional epibiont coverage (%) derived from drone (purple) and vessel-based (gold) imagery. Results are grouped by dorsal-surface anatomical regions: Tail flukes (n = 13), pectoral fins (n = 6), and rostra (n = 13). Jittered points denote individual observations, with whiskers extending to 1.5 times the interquartile range.

3.2.3 | Methodological and Biological Influences on Platform-Derived Estimates

Mean drone flight altitude for aerial samples used in the current study was 38.07 ± 1.07 m. The calculated GSD varied little across drone-derived image samples (mean = 1.53 ± 0.04 cm/px; range = 1.45–1.63 cm/px). Accordingly, GSD received less support as a fixed effect in both the beta GLMM for proportional epibiont coverage estimates and the Gaussian GLMM for log-transformed BIM pixel counts and was subsequently excluded from the final models (Table S1.2).

Model selection using AICc supported a beta regression GLMM including epibiont characteristics (attached barnacles vs. prior attachment scars), sampling method, time of day, and the interaction between method and time of day (AICc = −339.0, K = 7; Table S1.2). Fixed effects explained 23.3% of the variance, while the full model, including the Sample ID random effect, explained 92.0% of the variance. The adjusted ICC was 0.896, indicating substantial sample-level variability, with most variance attributable to differences among paired image samples (Table S1.3). The model showed that vessel-based image data yielded significantly lower proportional coverage than corresponding drone imagery ($\beta = -1.207$, SE = 0.297, $p < 0.001$; Table S1.3). It also indicated that skin showing predominantly barnacle scars resulted in significantly higher overall coverage estimates than attached organisms within this subsample ($\beta = 0.660$, SE = 0.272, $p = 0.015$; Table S1.3), a pattern consistent across the two imaging platforms. The interaction between the time of day when imagery was captured and the sampling method was significant ($\beta = 0.060$, SE = 0.025, $p = 0.018$; Table S1.3), with the difference between vessel- and drone-based estimates decreasing later in the day for both attached and scar detections (Figure 9).

3.2.4 | Comparative Analysis of Binary Image Mask Outputs by Platform

Pixel counts extracted from BIMs varied consistently across image sampling platforms, highlighting systematic differences in both segmented anatomical regions and epibiont-affected areas of humpback whale skin.

Model selection using AICc supported a Gaussian GLMM that excluded all two-way interactions. This model included the additive effects of BIM measurement type, age class, and time of day (AICc = 321.8, $K = 9$; Table S1.2). Fixed effects explained 90.1% of the variance, while the full model, including Sample ID as a random effect, explained 93.4%. The adjusted ICC was 0.330, indicating moderate among-individual variability, with some variance attributable to differences among paired image samples (Table S1.4). Later capture times were associated with lower pixel counts across all BIMs ($\beta = -0.074$, SE = 0.042, $p = 0.076$; Table S1.4).

Pixel counts for anatomical and epibiont ROIs consistently differed between image-acquisition platforms. Vessel-based BIMs yielded higher and more variable pixel counts than corresponding drone-derived BIMs (Table S1.4), especially for anatomical ROIs (range = 105,827–4,976,568 px). Specifically, pixel counts extracted from VBIM1 were significantly greater than those from the corresponding drone-derived mask type DBIM1 ($\beta = 3.593$, SE = 0.172, $p < 0.001$; Table S1.4). This was further supported by Tukey post hoc comparisons, which revealed that estimates from drone-derived anatomical ROIs (DBIM1; range = 4039–53,136 px) were significantly lower than those from vessel-based equivalents (estimate = −3.59, SE = 0.172, $_t119 = -20.89$, $p < 0.0001$; Table S1.5). Similarly, segmented epibiont ROIs (VBIM2 and DBIM2) showed significantly lower pixel counts in drone images compared to DSLR-derived images (estimate = −2.95, SE = 0.172, $_t119 = -17.13$, $p < 0.0001$; Table S1.5), further indicating systematic measurement biases associated with image-acquisition method (Figure 10).

Age class (whale size) significantly influenced mask pixel count regardless of mask measurement type. Adults ($\beta = 1.365$, SE = 0.292, $p < 0.001$; Table S1.4) and subadults ($\beta = 1.322$, SE = 0.233, $p < 0.001$; Table S1.4) consistently produced higher BIM pixel counts relative to calf counterparts (Figure 10). Estimated marginal means (EMMs) supported this trend, with log-transformed values increasing from calves (8.86% ± 0.16, 95% CI [8.60, 9.18]) to subadults (10.19% ± 0.17, 95% CI [9.85, 10.53]) and adults (10.23% ± 0.24, 95% CI [9.75, 10.71]). Consistent with the larger pixel counts observed for vessel-based anatomical ROIs, the strongest age-class effect was detected for VBIM1 (joint test: $F_{3,119} = 2648.85$, $p < 0.0001$).

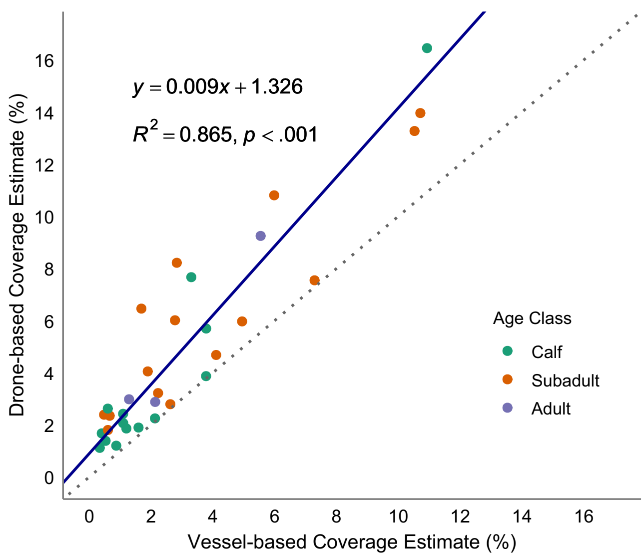

FIGURE 8 | Standard major axis (SMA) regression comparing pixel-based estimates of barnacle epibiont coverage (%) between drone and vessel-based images. Points are color-coded by age class: Calves (teal), subadults (orange), and adults (purple). The dashed gray line denotes a 1:1 reference slope.

4 | Discussion

In this study, we assessed the utility of drone-derived imagery for quantifying relative barnacle epibiont coverage on standardized dorsal-surface anatomical regions across age classes of breeding stock E1 humpback whales, using pairwise comparisons with conventional DSLR-based imaging. Drone imagery increased data availability across both study years and yielded more comprehensive and repeatable coverage estimates than corresponding vessel-based images of the same individuals. Although estimates from the two sampling platforms were strongly correlated, significant differences in their magnitude and consistency were evident. These differences appeared to be influenced by the interaction between time of day and image-capture method, with additional variation associated with the anatomical regions assessed and whale age class (size).

Across humpback whale age classes, drone imagery consistently yielded higher estimates of proportional epibiont coverage than vessel-based images, indicating a systematic sampling-platform effect. On average, vessel-based imagery captured only 58% of the proportional coverage recorded by corresponding drone imagery. Allometric scaling further indicated that the discrepancy between platforms increased as epibiont coverage increased, suggesting that vessel-based imagery increasingly underestimated coverage

TABLE 3 | Results of the one-tailed *t*-test performed on the proportional relationship between vessel- and drone-based epibiont coverage estimates, reported as the mean proportion of vessel-based estimates relative to paired drone-based estimates, with 95% confidence intervals (CIs).

Mean proportion ($\bar{X}$)	2.5% CI	97.5% CI	t	df	p
0.580	0.456	0.705	−9.7358	31	< 0.001

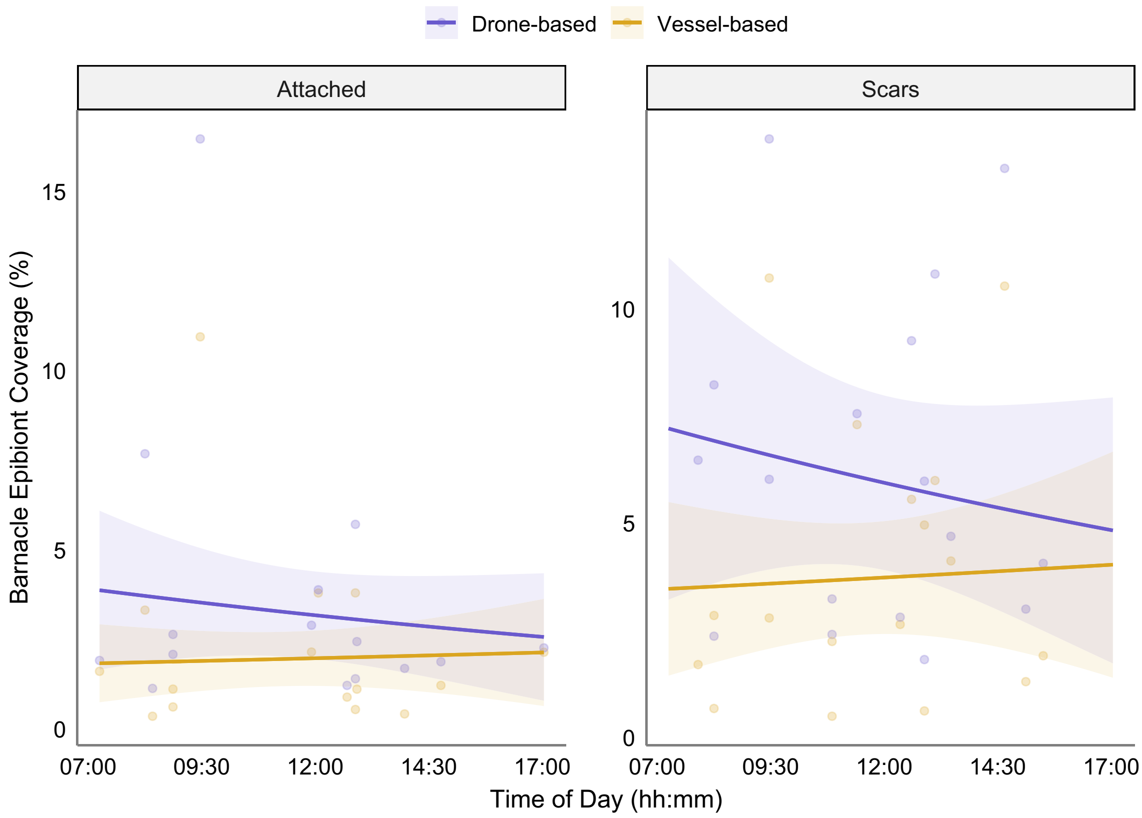

FIGURE 9 | Predicted barnacle epibiont coverage (%) on standardized humpback whale dorsal anatomies, based on a beta-regression generalized linear mixed model (GLMM). The interaction between image sampling platform (drone- vs. vessel-based) and time of capture (a proxy for solar position) is shown for imagery captured from 07:00 to 17:00 h. Estimates of proportional coverage derived from drone-based images are shown as purple lines, and estimates derived from vessel-based images are shown as gold lines. Shaded ribbons represent 95% confidence intervals, and colored points denote raw observations. Left: paired imagery with attached coronulid barnacles; right: paired imagery with barnacle scars.

at higher infestation levels. Despite these differences, 93.75% of paired observations fell within a 5% absolute-difference threshold (median = 1.29%), and most vessel-based samples (78.12%) had estimated proportional coverages below 5%. These findings suggest that although systematic measurement differences exist between platforms, they are unlikely to be ecologically significant for most assessments of humpback whale epibiont coverage. Overall, our study provides empirical support for the use of drone imagery as a repeatable, non-invasive method for quantifying epibionts, while demonstrating that vessel-based imagery provides broadly comparable estimates.

Platform-specific biases were evident in image-segmentation outcomes. Binary image masks derived from vessel-based imagery produced higher and more variable pixel counts than those for drone imagery, particularly for masks generated for anatomical landmarks. In contrast, equivalent masks generated from drone stills yielded lower but more consistent pixel counts. This likely reflects greater variability in the viewing angle and orientation of fluke images captured during surfacing events with DSLR cameras, which were often not perpendicular to the lens and sometimes included arching of the leading edges (e.g., during dives). Such variation can obscure or distort the visible surface area, leading to differences in pixel-based measurements when compared to the top-down perspectives provided by drones. In contrast, DSLR imagery more consistently captured dorsolateral rostral regions and near-perpendicular views of the pectoral fins, which may explain the smaller absolute differences in platform-based estimates of proportional epibiont coverage for these regions.

Discrepancies in proportional coverage estimates between the two imaging platforms were most pronounced during early morning captures. Compared to midday sampling, this time is associated with lower sun angles (i.e., solar elevations below 35°), which reduces reflectance back to drone sensors during over-water operations (Joyce et al. 2019; Mount 2005; Ramos et al. 2022), thereby minimizing the risk of oversaturation in light-colored pixels (Muslim et al. 2019). By contrast, even good-quality vessel-based images captured at near-perpendicular angles may have been susceptible to backlighting effects during this time (Urian et al. 2015), potentially obscuring light-colored barnacle-scar pixels during color-thresholding segmentation. Drone imagery collected at nadir can reduce variation in illumination and shadowing for a given sun angle, supporting more consistent exposure across the focal anatomical region (Joyce et al. 2019; Sekrecka et al. 2020). The top-down perspective provided by drone imagery may have enhanced the visibility of fine-scale features, such as barnacle scars, even under variable lighting conditions, suggesting a methodological advantage of drones for consistent quantitative epibiont assessment. Automatic exposure settings on the drone may also have contributed to platform-specific differences in image contrast and

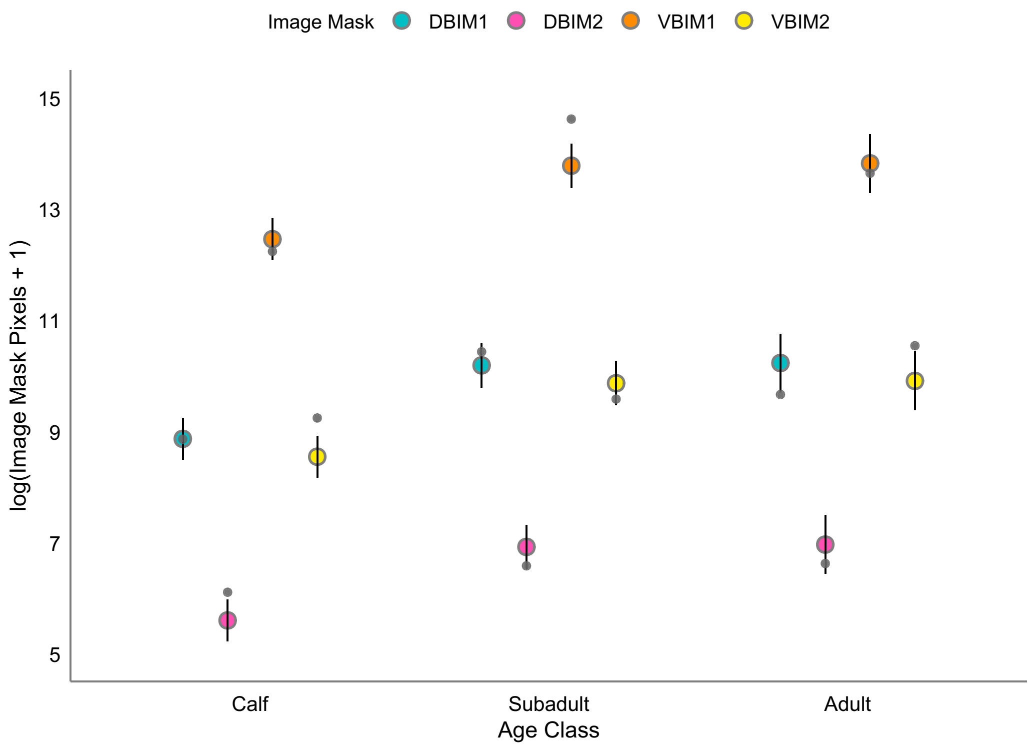

FIGURE 10 | Log-transformed pixel values from four binary image mask (BIM) measurement types (DBIM1: drone-based anatomy ROI; DBIM2: drone-based epibiont cover ROI; VBIM1: vessel-based anatomy ROI; VBIM2: vessel-based epibiont cover ROI) plotted by age class (calves, subadults, adults). Points show Gaussian GLMM-derived estimated marginal means (EMMs) for each mask type across age classes. Large colored circles indicate EMMs, and vertical lines indicate 95% confidence intervals. Smaller gray points represent the model-predicted values for individual observations.

therefore epibiont detection. However, only images meeting predefined quality criteria were included in the analysis. Together, these findings emphasize the importance of accounting for the time of day and solar elevation in cross-platform comparisons, as uncontrolled variation in these factors can introduce systematic biases in quantitative, pixel-based analyses (Sekrecka et al. 2020).

Drone-based imaging approaches are increasingly used to assess cetacean epidermal condition and document surface features used in individual identification (Bagchi et al. 2025; Evans et al. 2026; Lonati et al. 2022; O'Callaghan et al. 2024). Notably, Leslie et al. (2022) estimated dorsal-surface coverage of tattoo skin disease-like (TSD-L) lesions on Arabian Sea humpback whales using drone imagery and pixel-based proportional analysis, although they did not perform quantitative comparisons with vessel-based images of the same whale. Leslie et al. (2022) acknowledged that body curvature may lead to underestimation of lesion coverage in distal flank areas, thereby complicating quantitative comparisons with vessel-based images, whereas we applied standardized, comparable dorsal-surface anatomical references to improve the reliability of inter-platform estimates.

Despite our standardized approach, fully paired image datasets were not possible because of uncontrolled variables during vessel-based sampling. Although drone flight altitudes were relatively consistent, variability in vessel-based BIMs arose from several uncontrolled sampling factors, including the consistency in the orientation of anatomical landmarks, the angle between the observer and the whale at the time of image capture, vessel-to-whale proximity, and variation in effective image resolution associated with focal length/zoom position. Even after filtering vessel-based images by quality grade, such variability could not be entirely eliminated, underscoring the inherent challenges of standardizing pixel-based measurements from lateral observations (Toms et al. 2020). This limitation suggests that future comparative work may benefit from deriving a correction factor to adjust for systematic measurement discrepancies between platforms as preliminary datasets expand (Ramos et al. 2022). Nevertheless, overall epibiont-coverage patterns were discernible across both image-acquisition sources, and the magnitude of absolute differences between platforms was generally small. In the absence of a correction factor, estimates derived from either imagery type may therefore provide conservative minimum estimates of humpback whale epibiont coverage.

Both drone- and vessel-based sampling offer distinct advantages and limitations for assessing cetacean skin health and surface morphology. Drones can capture perpendicular imagery of the dorsal surface with substantially higher resolution than that obtained during costly, traditional crewed aerial surveys, which necessarily pass over animals at higher altitudes (Hamilton and Marx 2005; Hunt et al. 2013). In contrast, vessel-based platforms provide superior visibility in lateral views of cetacean appendages, the mouth, and distal body regions often obscured in aerial imagery (Minton et al. 2022; Ramp et al. 2021; Raoult et al. 2020). Each method entails trade-offs: drones may underestimate lateral areas, whereas obliquely angled vessel-based images can distort dorsal morphology (Leslie et al. 2022; Vilches et al. 2023). Nonetheless, vessel-based observations have provided valuable semi-quantitative information on health status and anthropogenic impacts, including the prevalence of entanglement scarring and assessments of body condition in some species (Hunt et al. 2013; Ramp et al. 2021). Furthermore, these observations have facilitated detailed views of macroscopic ectoparasites around the eyes and blowholes, as well as evaluations of parasitical prevalence (Boileau et al. 2024; Hermosilla et al. 2015; Pettis et al. 2004). However, variations in host physiology, surface exposure, and epibiont attachment sites—for instance, along the trailing edges of extremities and extending beyond anatomical landmarks—can complicate standardization in fully quantitative or proportional analyses of wild populations (Dolezal et al. 2023; Ten et al. 2025; Toms et al. 2020; Urian et al. 2019).

While we demonstrate that drone-derived imagery can reliably detect and quantify both existing and historical epibiont loads on the dorsal surfaces of humpback whales, several key limitations remain. The analysis relied on opportunistic data drawn from a broader dataset initially collected for photo-identification and body condition assessments. Consequently, the number of vessel-based images suitable for direct comparison with the available drone imagery was constrained, particularly for data collected before 2023, when documentation of dorsal surface anatomy, such as the head and extremities, was not a targeted objective. The absence of systematic variation in drone flight altitudes prevented an evaluation of altitude-related pixel measurement bias (e.g., Christie et al. 2022; Ramos et al. 2022). Furthermore, the small sample size, which was skewed toward calves and subadults, precluded robust demographic inference. As datasets expand, we anticipate that differences in epibiont attachment patterns across age classes and sexes will emerge, which were not detectable in the present study. Despite these limitations, the effectiveness of pixel-based techniques for assessing proportional epibiont coverage supports their incorporation into routine drone-based health assessments. Integrating image acquisition protocols into field activities may enhance the capacity for comparative demographic monitoring and enable more detailed longitudinal analyses of epibiont prevalence within and among populations. A significant implication of these limitations is the potential for demographic bias in epibiont assessments.

Vessel-based images of the anatomical landmarks used in this study were predominantly collected in Hervey Bay and were disproportionately unavailable for adult whales, limiting representation of this demographic in the paired dataset. Because this study relied on imagery collected opportunistically during concurrent research activities, consistently obtaining suitable vessel-based images of the rostrum and dorsal-surface regions of the appendages was also constrained. Behavioral differences among demographic groups likely contributed to these sampling limitations. For example, two of the six adult samples were from lactating females, which often spend extended periods resting at or near the surface (Franklin et al. 2021; Iwata et al. 2021). In the shallow waters of Hervey Bay, mothers with calves infrequently raise their tail flukes when diving (Stack et al. 2019), likely because the shallow environment reduces the need for steep dive angles and associated energetic expenditure (Bejder et al. 2019). Similar behavioral patterns have also been reported elsewhere for lactating humpback whales (Evans et al. 2026), further limiting opportunities to obtain standardized vessel-based images of the dorsal fluke surface. In contrast, although calves are larger in Hervey Bay than those occurring on breeding grounds, their less developed rostral region, combined with their highly surface-active behavior (Franklin et al. 2018, 2021), may have increased opportunities to capture the anatomical landmarks required for vessel-based analyses. Immature females and males (subadults) also display complex social interactions and non-agonistic behavior with non-lactating mature females in Hervey Bay (Franklin et al. 2021, 2012), facilitating more vessel-based observations from these cohorts. These findings highlight the value of complementary aerial footage, which was less constrained by demographic variation in behavior and broadened our observational capacity compared to DSLR imaging. Beyond improving epibiont assessments, rostral features such as tubercles and scars extracted from drone imagery can also provide a reliable means of identifying individuals when conventional fluke photographs cannot be obtained, thereby enhancing demographic coverage when documenting individual life histories in humpback whales (Evans et al. 2026; O'Mahony et al. 2024).

Although not the focus of this study, a comprehensive analysis of all available drone imagery from both years identified three additional calves documented in Hervey Bay that exhibited high juvenile coronulid barnacle coverage. Together with the calf rostrum sample included in the current analysis, these four individuals comprised 2% of the 184 calves surveyed using drone imagery over the two-year study period. For these additional encounters, vessel-based images were either unavailable or of insufficient quality, reinforcing the increased observational opportunities afforded by aerial sampling. High barnacle coverage (e.g., IE score of 3) on the anatomical landmarks used in this study was estimated at $\geq 10\%$ and $\geq 15\%$ in vessel- and drone-based samples, respectively. Based only on sufficient-quality drone-derived image samples, barnacle coverage on two additional calves was estimated at ~13% for the dorsal-side flukes and ~18% and ~29% for the rostra (Figures S4 and S5). Low levels of barnacle coverage appear to be typical of humpback whale populations studied to date. For example, Minton et al. (2022) found that 93% of Arabian Sea humpback whales exhibited $< 10\%$ barnacle coverage on the ventral flukes, with only one individual showing 10%–30% coverage. Although Minton et al. (2022) assessed a different anatomical region using qualitative scoring, whereas the present study quantified proportional coverage on dorsal anatomical regions, both studies indicate that extensive barnacle coverage is uncommon. While coronulids may increase drag (Fernando et al. 2006; Ten, Raga, and Aznar 2022), it is thought to have a relatively small impact on overall welfare (Geraci and Aubin 1987). Nonetheless, cases of high barnacle loading in calves remain rarely documented globally and warrant continued monitoring. The use of noninvasive tools such as drones offers a valuable means of detecting such events and investigating potential links between infestation prevalence and skin health (Boileau et al. 2024), particularly in early life stages.

Humpback whales exhibit variable ectoparasite and commensal interactions that vary with latitude, population, and migratory routes (Abollo et al. 1998; de Pina and Giuffra 2003; Elwen et al. 2014; Fransen and Smeenk 1991; Iwasa-Arai et al. 2017, 2018). This geographic diversity includes Arabian

Sea humpback whales, whose year-round residency likely influences epidermal conditions and associated epibiont assemblages (Mikhalev 1997; Minton et al. 2022). Consequently, standardized drone-based surveys incorporated into region-specific population health-monitoring frameworks will facilitate geographic comparisons. Coronulid barnacles are believed to spawn and settle in warmer waters, mature during host poleward migrations, and then shed after approximately 1 year (Angot 1951; Newman and Abbott 1980). Accordingly, sampling at lower latitudes is likely to be most informative for evaluating recent shedding, early attachment, and new colonization events, as reflected by the elevated barnacle-scar coverages and predominance of attached juvenile barnacles observed in our lower-latitude subsample of the E1 population. Targeted sampling of this population at higher latitudes would likely yield higher coverage estimates of attached *Coronula* spp., which can reach ~5 cm in diameter and 3 cm in height at maturity (Kim et al. 2020).

In the present study, the mean drone flight altitude was approximately 38 m. While no appreciable degradation in image quality was evident in the two samples acquired at ~40 m, image quality across flight altitudes was not formally assessed. The GSD (ground-level resolution) achieved during drone sampling was sufficient to detect sparse assemblages of coronulids and individual barnacle scars. However, finer resolution may be required to assess commensal densities, estimate their absolute abundance, or characterize epibiont morphology. While this study focused on relative proportional coverage—a metric we found to be well-suited to comparing epibiont coverage among individual whales across age classes and body sizes—quantifying the presence and abundance of indicator barnacles, such as *Xenobalanus globicipitis* (e.g., counts per unit length), may be especially informative in studies of smaller cetaceans (Carrillo et al. 2015; Ten et al. 2026, 2025; Ten, Konishi, et al. 2022). Such approaches would also reduce the need to restrict analyses to predefined anatomical surfaces, enabling the inclusion of epibiota occurring along cetacean appendage trailing edges and other external regions. Future work aiming to use altitude-based measurements in noninvasive assessments of epibiota should therefore incorporate a broader range of species-specific altitude treatments (e.g., ±10 m around our mean) and test different drone platforms to identify optimal resolutions for diverse epibiont–host systems (Andriolo et al. 2022, 2023; Ramos et al. 2022). However, species-specific adjustments are necessary to mitigate potential visual and acoustic disturbances during aerial sampling (e.g., Afridi et al. 2025; Castro et al. 2021; Lo et al. 2024; Russell et al. 2022; Smith et al. 2016).

We recommend expanding datasets to include larger sample sizes representing diverse cetacean host species, including different regional or migratory populations. Although our data included complex coastal backgrounds and the graph-cut segmentation approach performed well under those conditions, additional validation across a broader range of habitats and environmental backgrounds would further establish the general applicability of the workflow. Future initiatives focusing on physical measures of welfare should establish taxon- and application-specific drone flight altitudes that provide sufficient spatial resolution to consistently quantify dorsal epibiont coverage. This may, for example, facilitate the repeatable and unbiased assessment of advanced cyamid and diatom infections in large whales (Omura 1950; Ten, Raga, and Aznar 2022). A dorsal visual index (DVI), proposed by Leslie et al. (2022) and based on total visible pixels of the dorsal body, may also support comprehensive top-down assessments of ectoparasite infestations on humpback whales. For instance, whale lice (e.g., *Cyamus boopis*) can proliferate indiscriminately on entangled, injured, or immunosuppressed individuals with reduced motility, leading to perceived skin discoloration (Groch et al. 2018; Osmond and Kaufman 1998; Stack et al. 2024; Vargas-Castro et al. 2024). Because the present analysis relied on direct comparisons of platform-derived image measurements, post-processing adjustments were avoided to prevent potential alteration of visual features relevant to epibiont detection. Future studies may evaluate the use of standardized image-adjustment procedures; however, their suitability is likely to depend on the study context, target epibiont-host system, and analytical objectives. Additionally, subsurface imagery captured using UAVs could prove useful for quantifying ectoparasitic scarring and healing rates in rorquals, including those caused by cookiecutter shark (*Isistius* spp.) bites (Herr et al. 2023), thereby helping to address quantitative data deficiencies related to understudied or cryptic species (Best and Photopoulou 2016; Ramp et al. 2021; Ten, Raga, and Aznar 2022). However, the efficacy of drones in detecting subsurface hosts and their epibiota will depend critically on regional water clarity, as well as constraints related to sea state and time of image acquisition, including solar angle (Joyce et al. 2019; Ramos et al. 2022; Robinson and Visona-Kelly 2025).

5 | Conclusions

To the best of our knowledge, this study is the first to systematically compare drone imagery with conventional vessel-based imaging techniques for quantifying coverage of epibiota on dorsal surface anatomies of humpback whales. Despite the inherent challenges of evaluating paired image data from fundamentally different observational platforms, our findings demonstrate that drones provide a noninvasive, repeatable, and minimally biased platform for quantitative assessments of epibiotic load on individual humpback whales. This was supported by low variance in our repeated pixel-based measurements (< 1%). Pixel-based proportional analysis applied to drone stills offered an effective and standardized method for assessing dorsal epibiont coverage, applicable across age classes. The approach is particularly well suited to demographic groups sensitive to disturbance, such as mother–calf pairs, and has potential for applicability to other cetacean species. The integration of drone-based epibiont assessments into broader research programs may enable efficient inferences on anthropogenic impacts, particularly for assessing the prolonged effects of entanglement, vessel collisions, and habitat degradation, and inform conservation strategies (Boileau et al. 2024; Correia et al. 2023; Hanninger et al. 2023; Minton et al. 2022).

Drones are likely to supplement, not supplant, vessel-based imaging techniques in comprehensive evaluations of epibiont–host interactions in large whales. For example, ventral surfaces, less commonly captured during drone sampling, include primary attachment sites for barnacle epibionts in humpback whales, such as throat pleats and the genital aperture

(Newman and Abbott 1980). Nonetheless, aerial sampling of standardized dorsal regions may be selected based on study objectives and logistical constraints without introducing significant ecological bias. However, transitioning between platforms can introduce systematic differences in coverage estimates, necessitating calibration studies to reduce bias in time-series analyses. The accepted threshold (5% absolute difference) between sampling platform estimates of coverage may be insufficient for accurately evaluating cetacean lesions of unknown etiologies or emerging diseases (Toms et al. 2020; Vargas-Castro et al. 2024). Finally, as drone technology and autonomous detection systems continue to evolve, we anticipate that quantitative aerial assessments of epibiont–host interactions—combined with other complementary measures like virological surveillance via blow sampling (Sekine et al. 2025)—will become an integral component of cetacean population health monitoring programs.

Author Contributions

Barry McGovern: supervision, writing – review and editing, conceptualization, investigation. **Stephanie H. Stack:** writing – review and editing, conceptualization, funding acquisition, investigation, supervision. **Ticiana Fettermann:** data curation, writing – review and editing, investigation. **David S. Schoeman:** formal analysis, writing – review and editing, supervision. **Adrian B. McCallum:** funding acquisition, methodology, writing – review and editing, software, resources, supervision. **Isabel A. R. Taylor:** conceptualization, formal analysis, visualization, writing – original draft, writing – review and editing, investigation, methodology, project administration, validation.

Acknowledgments

The authors acknowledge the Butchulla and Thaua peoples as the Traditional Custodians of the Land, Sea, and Sky Country on which this research was conducted. We thank the Pacific Whale Foundation (PWF) and the University of the Sunshine Coast for providing funding support for this project. We are grateful to Emily Gregory, Teresa Hipolito, Rhian Bland, Nina Rothe, Leanne Nguyen, Carla Patulny, and Tine Haslam Nielsen for their assistance collecting UAV data. We additionally thank the many staff and volunteers who have contributed to Pacific Whale Foundation's long-term research efforts in Australia. We also sincerely appreciate the thoughtful feedback and constructive suggestions provided by the journal editors, Drs. Daryl Boness and Ari Friedlaender, and the anonymous Reviewers on earlier versions of this manuscript. Open access publishing facilitated by Griffith University, as part of the Wiley - Griffith University agreement via the Council of Australasian University Librarians.

Funding

This work was supported by the Pacific Whale Foundation (PWF) and the University of the Sunshine Coast.

Conflicts of Interest

The authors declare no conflicts of interest.

Data Availability Statement

The code supporting the findings of this study is available from the corresponding author upon reasonable request. The data supporting the findings of this study are owned by the Pacific Whale Foundation and are not publicly archived; access requests should be directed to the Research Program Director at research@pacificwhale.org.

References

Abollo, E., A. López, C. Gestal, P. Benavente, and S. Pascual. 1998. "Macroparasites in Cetaceans Stranded on the Northwestern Spanish Atlantic Coast." *Diseases of Aquatic Organisms* 32, no. 3: 227–231.

Afridi, S., L. Laporte-Devylder, G. Maalouf, et al. 2025. "Impact of Drone Disturbances on Wildlife: A Review." *Drones* 9, no. 4: 311.

Aguilar, A., and J. A. Raga. 1993. "The Striped Dolphin Epizootic in the Mediterranean Sea." *Ambio* 22, no. 8: 524–528.

Álvarez-González, M., P. Suarez-Bregua, G. J. Pierce, and C. Saavedra. 2023. "Unmanned Aerial Vehicles (UAVs) in Marine Mammal Research: A Review of Current Applications and Challenges." *Drones* 7, no. 11: 667.

Anderson, D., K. Burnham, and G. White. 1994. "AIC Model Selection in Overdispersed Capture-Recapture Data." *Ecology* 75, no. 6: 1780–1793.

Andrews-Goff, V., S. Bestley , N. J. Gales, et al. 2018. "Humpback Whale Migrations to Antarctic Summer Foraging Grounds through the Southwest Pacific Ocean." *Scientific Reports* 8, no. 1: 12333. https://doi.org/10.1038/s41598-018-30748-4.

Andriolo, U., O. Garcia-Garin, M. Vighi, A. Borrell, and G. Gonçalves. 2022. "Beached and Floating Litter Surveys by Unmanned Aerial Vehicles: Operational Analogies and Differences." *Remote Sensing* 14, no. 6: 1336.

Andriolo, U., K. Topouzelis, T. H. M. van Emmerik, et al. 2023. "Drones for Litter Monitoring on Coasts and Rivers: Suitable Flight Altitude and Image Resolution." *Marine Pollution Bulletin* 195: 115521. https://doi.org/10.1016/j.marpolbul.2023.115521.

Angliss, R., M. Ferguson, P. Hall, V. Helker, A. Kennedy, and T. Sformo. 2018. "Comparing Manned to Unmanned Aerial Surveys for Cetacean Monitoring in the Arctic: Methods and Operational Results." *Journal of Unmanned Vehicle Systems* 6, no. 3: 109–127.

Angot, M. 1951. "Rapport Scientifique Sur Les Expeditions Baleinieres Autour de Madagascar (Saisons 1949 et 1950)."

Aoki, K., S. Isojunno, C. Bellot, et al. 2021. "Aerial Photogrammetry and Tag-Derived Tissue Density Reveal Patterns of Lipid-Store Body Condition of Humpback Whales on Their Feeding Grounds." *Proceedings of the Royal Society B: Biological Sciences* 288, no. 1943: 20202307. https://doi.org/10.1098/rspb.2020.2307.

Arel-Bundock, V., N. Greifer, and A. Heiss. 2024. "How to Interpret Statistical Models Using Marginaleffects for R and Python." *Journal of Statistical Software* 111: 1–32.

Atkinson, S., A. Rogan, C. S. Baker, et al. 2021. "Genetic, Endocrine, and Microbiological Assessments of Blue, Humpback and Killer Whale Health Using Unoccupied Aerial Systems." *Wildlife Society Bulletin* 45, no. 4: 654–669.

Aznar, F., M. Fernández, and J. Balbuena. 2010. "Why We Should Care About the Parasite Fauna of Cetaceans: A Plea for Integrative Studies." In *Whales and Dolphins: Behavior, Biology, and Distribution*, 811–820. Nova Science Publishers.

Aznar, F. J., D. Perdiguero, A. Perez del Olmo, A. Repulles, C. Agusti, and J. A. Raga. 2005. "Changes in Epizoic Crustacean Infestations During Cetacean Die-Offs: The Mass Mortality of Mediterranean Striped Dolphins *Stenella coeruleoalba* Revisited." *Diseases of Aquatic Organisms* 67, no. 3: 239–247. https://doi.org/10.3354/dao067239.

Bagchi, C., J. Medina, D. J. Irschick, S. Maji, and F. Christiansen. 2025. "Automated Extraction of Right Whale Morphometric Data From Drone Aerial Photographs." *Remote Sensing in Ecology and Conservation* 11, no. 4: 438–453. https://doi.org/10.1002/rse2.70001.

Bartoń, K. 2024. "MuMIn: Multi-Model Inference (Version R Package Version 1.48.4)." https://cran.r-project.org/package=MuMIn.

Bejder, L., S. Videsen, L. Hermannsen, M. Simon, D. Hanf, and P. Madsen. 2019. "Low Energy Expenditure and Resting Behaviour of Humpback Whale Mother-Calf Pairs Highlights Conservation Importance of Sheltered Breeding Areas." *Scientific Reports* 9, no. 1: 771.

Bejder, M., D. W. Johnston, J. Smith, A. Friedlaender, and L. Bejder. 2016. "Embracing Conservation Success of Recovering Humpback Whale Populations: Evaluating the Case for Downlisting Their Conservation Status in Australia." *Marine Policy* 66: 137–141.

Best, P. B., and T. Photopoulou. 2016. "Identifying the 'Demon Whale-Biter': Patterns of Scarring on Large Whales Attributed to a Cookie-Cutter Shark Isistius sp." *PLoS One* 11, no. 4: e0152643.

Boileau, A., J. Blais, M.-F. Van Bressem, K. E. Hunt, and J. Ahloy-Dallaire. 2024. "Physical Measures of Welfare in Fin (*Balaenoptera physalus*) and Humpback Whales (Megaptera Novangliae) Found in an Anthropized Environment: Validation of a First Animal-Based Indicator in Mysticetes." *Animals: An Open Access Journal From MDPI* 14, no. 23: 3519.

Bora, D. J., A. K. Gupta, and F. A. Khan. 2015. "Comparing the Performance of L*A*B* and HSV Color Spaces With Respect to Color Image Segmentation." *arXiv Preprint* arXiv:1506.01472.

Bortolotto, G. A., L. Thomas, P. Hammond, and A. N. Zerbini. 2021. "Alternative Method for Assessment of Southwestern Atlantic Humpback Whale Population Status." *PLoS One* 16, no. 11: e0259541.

Bradford, A. L., D. W. Weller, A. M. Burdin, and J.,. R. L. Brownell. 2011. "Using Barnacle and Pigmentation Characteristics to Identify Gray Whale Calves on Their Feeding Grounds." *Marine Mammal Science* 27, no. 3: 644–651.

Bradford, A. L., D. W. Weller, A. E. Punt, et al. 2012. "Leaner Leviathans: Body Condition Variation in a Critically Endangered Whale Population." *Journal of Mammalogy* 93, no. 1: 251–266. https://doi.org/10.1644/11-mamm-a-091.1.

Briggs, K., and G. V. Morejohn. 1972. "Barnacle Orientation and Water Flow Characteristics in California Grey Whales." *Journal of Zoology* 167, no. 3: 287–292.

Brooks, L., T. Franklin, W. Franklin, P. Harrison, P. Corkeron, and K. H. Pollock. 2024. "Humpback Whales (*Megaptera novaeangliae*) in Hervey Bay, Australia: A Stopover for Females Early in Their Southern Migration." *Frontiers in Marine Science* 11: 1426248.

Brooks, M. E., K. Kristensen, K. J. V. Benthem, et al. 2017. "glmmTMB Balances Speed and Flexibility Among Packages for Zero-Inflated Generalized Linear Mixed Modeling." *R Journal* 9: 378.

Burnett, J. D., L. Lemos, D. Barlow, M. G. Wing, T. Chandler, and L. G. Torres. 2019. "Estimating Morphometric Attributes of Baleen Whales With Photogrammetry From Small UASs: A Case Study With Blue and Gray Whales." *Marine Mammal Science* 35, no. 1: 108–139. https://doi.org/10.1111/mms.12527.

Burns, D., L. Brooks, P. Harrison, et al. 2014. "Migratory Movements of Individual Humpback Whales Photographed Off the Eastern Coast of Australia." *Marine Mammal Science* 30, no. 2: 562–578.

Bushuev, S. 1990. "A Study of the Population Structure of the Southern Minke Whale (*Balaenoptera acutorostrata* Lacépède) Based on Morphological and Ecological Variability." *Report of the International Whaling Commission* 40: 317–324.

Calambokidis, J., E. A. Falcone, T. J. Quinn, et al. 2008. "SPLASH: Structure of Populations, Levels of Abundance and Status of Humpback Whales in the North Pacific." C. R. Final Report for Contract AB133F-03-RP-00078.

Carrillo, J. M., R. M. Overstreet, J. A. Raga, and F. J. Aznar. 2015. "Living on the Edge: Settlement Patterns by the Symbiotic Barnacle *Xenobalanus globicipitis* on Small Cetaceans." *PLoS One* 10, no. 6: e0127367.

Cartwright, R., and M. Sullivan. 2009. "Behavioral Ontogeny in Humpback Whale (*Megaptera novaeangliae*) Calves During Their Residence in Hawaiian Waters." *Marine Mammal Science* 25, no. 3: 659–680. https://doi.org/10.1111/j.1748-7692.2009.00286.x.

Castrillon, J., and S. Bengtson Nash. 2020. "Evaluating Cetacean Body Condition; a Review of Traditional Approaches and New Developments." *Ecology and Evolution* 10, no. 12: 6144–6162.

Castro, J., F. O. Borges, A. Cid, M. I. Laborde, R. Rosa, and H. C. Pearson. 2021. "Assessing the Behavioural Responses of Small Cetaceans to Unmanned Aerial Vehicles." *Remote Sensing* 13, no. 1: 156.

Chaloupka, M., and M. Osmond. 1999. "Spatial and Seasonal Distribution of Humpback Whales in the Great Barrier Reef." In *Life in the Slow Lane: Ecology and Conservation of Long-Lived Marine Animals*, edited by J. A. Musick, vol. 23, 89–106. American Fisheries Society.

Cheney, B. J., J. Dale, P. M. Thompson, and N. J. Quick. 2022. "Spy in the Sky: A Method to Identify Pregnant Small Cetaceans." *Remote Sensing in Ecology and Conservation* 8, no. 4: 492–505.

Chittleborough, R. 1965. "Dynamics of Two Populations of the Humpback Whale, *Megaptera novaeangliae* (Borowski)." *Marine and Freshwater Research* 16, no. 1: 33–128.

Christiansen, F., A. M. Dujon, K. R. Sprogis, J. P. Y. Arnould, and L. Bejder. 2016. "Noninvasive Unmanned Aerial Vehicle Provides Estimates of the Energetic Cost of Reproduction in Humpback Whales." *Ecosphere* 7, no. 10: e01468. https://doi.org/10.1002/ecs2.1468.

Christiansen, F., M. L. Nielsen, C. Charlton, L. Bejder, and P. T. Madsen. 2020. "Southern Right Whales Show no Behavioral Response to Low Noise Levels From a Nearby Unmanned Aerial Vehicle." *Marine Mammal Science* 36, no. 3: 953–963.

Christiansen, F., K. R. Sprogis, J. Gross, et al. 2020. "Variation in Outer Blubber Lipid Concentration Does Not Reflect Morphological Body Condition in Humpback Whales." *Journal of Experimental Biology* 223, no. 8: jeb.213769. https://doi.org/10.1242/jeb.213769.

Christiansen, F., F. Vivier, C. Charlton, et al. 2018. "Maternal Body Size and Condition Determine Calf Growth Rates in Southern Right Whales." *Marine Ecology Progress Series* 592: 267–281. https://www.int-res.com/abstracts/meps/v592/p267-281/.

Christie, A. I., A. P. Colefax, and D. Cagnazzi. 2022. "Feasibility of Using Small UAVs to Derive Morphometric Measurements of Australian Snubfin (*Orcaella heinsohni*) and Humpback (*Sousa sahulensis*) Dolphins." *Remote Sensing* 14, no. 1: 21.

Clapham, P. J., and J. G. Mead. 1999. "*Megaptera novaeangliae*." *Mammalian Species* 604: 1–9. https://doi.org/10.2307/3504352.

Clapham, P., Y. Mikhalev, W. Franklin, et al. 2009. "Catches of Humpback Whales, *Megaptera novaeangliae*, by the Soviet Union and Other Nations in the Southern Ocean, 1947–1973."

Clapham, P. J., S. B. Young, and R. L. Brownell Jr. 1999. "Baleen Whales: Conservation Issues and the Status of the Most Endangered Populations." *Mammal Review* 29, no. 1: 37–62.

Clarke, R. 1966. "The Stalked Barnacle Conchoderma, Ectoparasitic on Whales." *Norsk Hvalfangst-Tidende* 55: 153–168.

Correia, A. M., E. Dietterle, A. Dinis, and F. Alves. 2023. "Defining a Common Language to Assess External Deformities in Free-Ranging Cetaceans." *Mammal Review* 53, no. 3: 189–205.

Costa, H., A. Rogan, C. Zadra, O. Larsen, A. H. Rikardsen, and C. Waugh. 2022. "Blowing in the Wind: Using a Consumer Drone for the Collection of Humpback Whale (*Megaptera novaeangliae*) Blow Samples During the Arctic Polar Nights." *Drones* 7, no. 1: 15.

Currie, J. J., M. van Aswegen, S. H. Stack, K. L. West, F. Vivier, and L. Bejder. 2021. "Rapid Weight Loss in Free Ranging Pygmy Killer Whales (*Feresa attenuata*) and the Implications for Anthropogenic Disturbance of Odontocetes." *Scientific Reports* 11, no. 1: 8181. https://doi.org/10.1038/s41598-021-87514-2.

Das, K., G. Malarvannan, A. Dirtu, et al. 2017. "Linking Pollutant Exposure of Humpback Whales Breeding in the Indian Ocean to Their Feeding Habits and Feeding Areas Off Antarctica." *Environmental Pollution* 220: 1090–1099.

Dawbin, W. 1966. "The Seasonal Migratory Cycle of Humpback Whales." In *Whales, Dolphins and Porpoises*. University of California Press.

Dawson, S. M., M. H. Bowman, E. Leunissen, and P. Sirguey. 2017. "Inexpensive Aerial Photogrammetry for Studies of Whales and Large Marine Animals [Methods]." *Frontiers in Marine Science* 4: 366. https://doi.org/10.3389/fmars.2017.00366.

de Pina, G. A., and R. Giuffra. 2003. "Taxonomía, Distribución y Notas Sobre Cuatro Especies de Ectoparásitos de Cetacea (Crustacea: Amphipoda: Cyamidae)." *Revista Del Museo Argentino de Ciencias Naturales* 5, no. 1: 39–62.

Delignette-Muller, M. L., and C. Dutang. 2015. "Fitdistrplus: An R Package for Fitting Distributions." *Journal of Statistical Software* 64, no. 4: 1–34. https://doi.org/10.18637/jss.v064.i04.

Dickens, J., P. R. Hollyman, T. Hart, et al. 2021. "Developing UAV Monitoring of South Georgia and the South Sandwich Islands' Iconic Land-Based Marine Predators." *Frontiers in Marine Science* 8: 654215.

Dickson, T., W. Rayment, and S. Dawson. 2021. "Drone Photogrammetry Allows Refinement of Acoustically Derived Length Estimation for Male Sperm Whales." *Marine Mammal Science* 37, no. 3: 1150–1158.

Dolezal, M. M., V. Foroughirad, F. E. Fish, et al. 2023. "Some Like It Hot: Temperature and Hydrodynamic Factors Influence *Xenobalanus globicipitis* Attachment to Cetaceans." *Marine Mammal Science* 39, no. 3: 961–975.

Durban, J. W., M. J. Moore, G. Chiang, et al. 2016. "Photogrammetry of Blue Whales With an Unmanned Hexacopter." *Marine Mammal Science* 32, no. 4: 1510–1515. https://doi.org/10.1111/mms.12328.

Ejrnæs, D. D., and K. R. Sprogis. 2021. "Ontogenetic Changes in Energy Expenditure and Resting Behaviour of Humpback Whale Mother–Calf Pairs Examined Using Unmanned Aerial Vehicles." *Wildlife Research* 49, no. 1: 34–45.

Elwen, S. H., N. Tonachella, J. Barendse, et al. 2014. "Humpback Whales Off Namibia: Occurrence, Seasonality, and a Regional Comparison of Photographic Catalogs and Scarring." *Journal of Mammalogy* 95, no. 5: 1064–1076.

Evans, L. I., M. van Aswegen, S. Feinberg, et al. 2026. "Elevating Photo-Identification: Aerial-Identification Improves re-Sight Rates and Supports Long-Term Monitoring of Humpback Whales." *Marine Mammal Science* 42, no. 1: e70078.

Fernando, F., B. Bearson, and J. Falconí. 2006. "Epizoic Barnacles Removed From the Skin of a Humpback Whale After a Period of Intense Surface Activity." *Marine Mammal Science* 22, no. 4: 979–984.

Fertl, D., and W. A. Newman. 2018. "Barnacles." In *Encyclopedia of Marine Mammals*, 75–78. Elsevier.

Fettermann, T., L. Fiori, L. Gillman, K. A. Stockin, and B. Bollard. 2022. "Drone Surveys Are More Accurate Than Boat-Based Surveys of Bottlenose Dolphins (*Tursiops truncatus*)." *Drones* 6, no. 4: 82.

Fish, F. E., and J. M. Battle. 1995. "Hydrodynamic Design of the Humpback Whale Flipper." *Journal of Morphology* 225, no. 1: 51–60.

Franklin, T., L. O. Brooks, W. Franklin, et al. 2020. "Photo-Identification of Individual Humpback Whales (*Megaptera novaeangliae*) Using All Available Natural Marks: Implications for Misidentification and Automated Algorithm Matching Technology." *Journal of Cetacean Research and Management* 21, no. 1: 71–83.

Franklin, T., W. Franklin, L. Brooks, and P. Harrison. 2018. "Site-Specific Female-Biased Sex Ratio of Humpback Whales (*Megaptera novaeangliae*) During a Stopover Early in the Southern Migration." *Canadian Journal of Zoology* 96, no. 6: 533–544.

Franklin, T., W. Franklin, L. Brooks, P. Harrison, A. A. Pack, and P. J. Clapham. 2021. "Social Behaviour of Humpback Whales (*Megaptera novaeangliae*) in Hervey Bay, Eastern Australia, a Preferential Female Stopover During the Southern Migration [Original Research]." *Frontiers in Marine Science* 8: 652147. https://doi.org/10.3389/fmars.2021.652147.

Franklin, W., T. Franklin, L. Brooks, et al. 2012. "Antarctic Waters (Area V) Near the Balleny Islands Are a Summer Feeding Area for Some Eastern Australian Breeding Stock E (i) Humpback Whales (*Megaptera novaeangliae*)." *Journal of Cetacean Research and Management* 12, no. 3: 321–327.

Fransen, C., and C. Smeenk. 1991. "Whale-Lice (Amphipoda: Cyamidae) Recorded From the Netherlands." *Zoologische Mededelingen* 65, no. 29: 393–405.

Garcia-Garin, O., A. Aguilar, A. Borrell, et al. 2020. "Who's Better at Spotting? A Comparison Between Aerial Photography and Observer-Based Methods to Monitor Floating Marine Litter and Marine Mega-Fauna." *Environmental Pollution* 258: 113680. https://doi.org/10.1016/j.envpol.2019.113680.

Geraci, J. R., and D. J. S. Aubin. 1987. "Effects of Parasites on Marine Mammals." *International Journal for Parasitology* 17, no. 2: 407–414.

Geraci, J. R., and V. J. Lounsbury. 2005. *Marine Mammals Ashore: A Field Guide for Strandings*. National Aquarium in Baltimore.

Glarou, M., S. Gero, A. Frantzis, et al. 2023. "Estimating Body Mass of Sperm Whales From Aerial Photographs." *Marine Mammal Science* 39, no. 1: 251–273. https://doi.org/10.1111/mms.12982.

Goebel, M. E., W. L. Perryman, J. T. Hinke, et al. 2015. "A Small Unmanned Aerial System for Estimating Abundance and Size of Antarctic Predators." *Polar Biology* 38: 619–630.

Groch, K. R., J. Díaz-Delgado, M. C. Marcondes, et al. 2018. "Pathology and Causes of Death in Stranded Humpback Whales (*Megaptera novaeangliae*) From Brazil." *PLoS One* 13, no. 5: e0194872.

Grolemund, G., and H. Wickham. 2011. "Dates and Times Made Easy With Lubridate." *Journal of Statistical Software* 40, no. 3: 1–25. https://doi.org/10.18637/jss.v040.i03.

Hamilton, P. K., and M. K. Marx. 2005. "Skin Lesions on North Atlantic Right Whales: Categories, Prevalence and Change in Occurrence in the 1990s." *Diseases of Aquatic Organisms* 68, no. 1: 71–82.

Hanninger, E.-M., J. Selling, K. Heyer, and P. Burkhardt-Holm. 2023. "Skin Conditions, Epizoa, Ectoparasites and Emaciation in Cetaceans in the Strait of Gibraltar: An Update for the Period 2016-2020." *Journal of Cetacean Research and Management* 24, no. 1: 121–142.

Hauser, N., A. N. Zerbini, Y. Geyer, M.-P. Heide-Jørgensen, and P. Clapham. 2010. "Movements of Satellite-Monitored Humpback Whales, *Megaptera novaeangliae*, From The Cook Islands." *Marine Mammal Science* 26, no. 3: 679–685.

Hermosilla, C., L. M. R. Silva, R. Prieto, S. Kleinertz, A. Taubert, and M. A. Silva. 2015. "Endo- and Ectoparasites of Large Whales (Cetartiodactyla: Balaenopteridae, Physeteridae): Overcoming Difficulties in Obtaining Appropriate Samples by Non- and Minimally-Invasive Methods." *International Journal for Parasitology: Parasites and Wildlife* 4, no. 3: 414–420. https://doi.org/10.1016/j.ijppaw.2015.11.002.

Herr, H., P. Burkhardt-Holm, K. Heyer, U. Siebert, and J. Selling. 2020. "Injuries, Malformations, and Epidermal Conditions in Cetaceans of the Strait of Gibraltar." *Aquatic Mammals* 46, no. 2: 215–235.

Herr, H., S. Viquerat, T. Naujocks, B. Gregory, A. Lees, and F. Devas. 2023. "Skin Condition of Fin Whales at Antarctic Feeding Grounds Reveals Little Evidence for Anthropogenic Impacts and High Prevalence of Cookiecutter Shark Bite Lesions." *Marine Mammal Science* 39, no. 1: 299–310. https://doi.org/10.1111/mms.12966.

Hodgson, A., N. Kelly, and D. Peel. 2013. "Unmanned Aerial Vehicles (UAVs) for Surveying Marine Fauna: A Dugong Case Study." *PLoS One* 8, no. 11: e79556.

Hodgson, J. C., D. Holman, A. Terauds, L. P. Koh, and S. D. Goldsworthy. 2020. "Rapid Condition Monitoring of an Endangered Marine Vertebrate Using Precise, Non-Invasive Morphometrics." *Biological Conservation* 242: 108402. https://doi.org/10.1016/j.biocon.2019.108402.

Horton, T. W., A. N. Zerbini, A. Andriolo, D. Danilewicz, and F. Sucunza. 2020. "Multi-Decadal Humpback Whale Migratory Route Fidelity Despite Oceanographic and Geomagnetic Change." *Frontiers in Marine Science* 7: 414.

Hunt, K. E., M. J. Moore, R. M. Rolland, et al. 2013. "Overcoming the Challenges of Studying Conservation Physiology in Large Whales: A Review of Available Methods." *Conservation Physiology* 1, no. 1: cot006.

International Whaling Commission. 2020. "Report of the IWC Workshop on Marine Debris: The Way Forward."

Iwasa-Arai, T., F. da Silva Santana, C. B. Barbosa, and M. R. Werneck. 2021. "One Crawled Over the Dolphin's Back: Unusual Record of the Whale Louse *Cyamus boopis* (Crustacea: Amphipoda: Cyamidae) on the Bottlenose Dolphin (*Tursiops truncatus*)." *Zoologischer Anzeiger* 295: 117–119.

Iwasa-Arai, T., A. S. Freire, A. C. Colosio, and C. S. Serejo. 2017. "Ontogenetic Development and Redescription of the Whale Louse *Cyamus boopis* Lütken, 1870 (Crustacea: Amphipoda: Cyamidae), Ectoparasite of Humpback Whale *Megaptera novaeangliae* (Mammalia: Cetacea: Balaenopteridae)." *Marine Biodiversity* 47, no. 3: 929–939. https://doi.org/10.1007/s12526-016-0532-z.

Iwasa-Arai, T., C. S. Serejo, S. Siciliano, et al. 2018. "The Host-Specific Whale Louse (*Cyamus boopis*) as a Potential Tool for Interpreting Humpback Whale (*Megaptera novaeangliae*) Migratory Routes." *Journal of Experimental Marine Biology and Ecology* 505: 45–51.

Iwata, T., M. Biuw, K. Aoki, P. J. O. Miller, and K. Sato. 2021. "Using an Omnidirectional Video Logger to Observe the Underwater Life of Marine Animals: Humpback Whale Resting Behaviour." *Behavioural Processes* 186: 104369.

Johnson, C. M., R. R. Reisinger, D. M. Palacios, et al. 2022. *Protecting Blue Corridors-Challenges and Solutions for Migratory Whales Navigating National and International Seas*. World Wildlife Fund.

Johnston, D. R., W. Rayment, and S. M. Dawson. 2022. "Morphometrics and Body Condition of Southern Right Whales on the Calving Grounds at Port Ross, Auckland Islands." *Mammalian Biology* 102, no. 4: 1525–1536.

Jones, L. S., T. A. Stephenson, A. M. Zoidis, and S. K. Todd. 2022. "Drone Observations of a Mother–Calf Humpback Whale (*Megaptera novaeangliae*) Pair Synchronous Feeding in the Bay of Fundy, Canada." *Aquatic Mammals* 48, no. 6: 716–719.

Joyce, K. E., S. Duce, S. M. Leahy, J. Leon, and S. W. Maier. 2019. "Principles and Practice of Acquiring Drone-Based Image Data in Marine Environments." *Marine and Freshwater Research* 70, no. 7: 952–963. https://doi.org/10.1071/MF17380.

Kaliszewska, Z. A., J. Seger, V. J. Rowntree, et al. 2005. "Population Histories of Right Whales (Cetacea: Eubalaena) Inferred From Mitochondrial Sequence Diversities and Divergences of Their Whale Lice (Amphipoda: Cyamus)." *Molecular Ecology* 14, no. 11: 3439–3456.

Kasuya, T., and D. Rice. 1970. *Notes on Baleen Plates and on Arrangement of Parasitic Barnacles of Gray Whale*. Vol. 22, 39–43. Scientific Reports of the Whales Research Institute.

Kaufman, G., D. Coughran, J. M. Allen, et al. 2011. *Photographic Evidence of Interchange Between East Australia (BS E-1) and West Australia (BS–D) Humpback Whale Breeding Populations*. Vol. 16. Scientific Committee of the International Whaling Commission SC63/SH11.

Kaufman, G., M. Smultea, and P. Forestell. 1987. "Use of Lateral Body Pigmentation Patterns for Photographic Identification of East Australian (Area V) Humpback Whales." *Cetus* 7, no. 1: 5–13.

Keeling, S. E., C. Napoli, J. Meza-Fidalgo, et al. 2025. "Drone-Based Observations of Scarring Patterns in Humpback Whales (*Megaptera novaeangliae*) in the New York Bight Provide Insight Into Foraging Behavior and Anthropogenic Threats." *PLoS One* 20, no. 5: e0324121.

Kim, H. K., B. K. Chan, C.-B. Kang, H. W. Kim, and W. Kim. 2020. "How Do Whale Barnacles Live on Their Hosts? Functional Morphology and Mating-Group Sizes of *Coronula diadema* (Linnaeus, 1767) and *Conchoderma auritum* (Linnaeus, 1767) (Cirripedia: Thoracicalcarea)." *Journal of Crustacean Biology* 40, no. 6: 808–824.

Koski, W. R., G. Gamage, A. R. Davis, T. Mathews, B. LeBlanc, and S. H. Ferguson. 2015. "Evaluation of UAS for Photographic Re-Identification of Bowhead Whales, *Balaena mysticetus*." *Journal of Unmanned Vehicle Systems* 3, no. 1: 22–29.

Landeo-Yauri, S. S., E. A. Ramos, D. N. Castelblanco-Martínez, C. A. Niño-Torres, and L. Searle. 2020. "Using Small Drones to Photo-Identify Antillean Manatees: A Novel Method for Monitoring an Endangered Marine Mammal in the Caribbean Sea." *Endangered Species Research* 41: 79–90.

Lenth, R. V. 2024. "Emmeans: Estimated Marginal Means, Aka Least-Squares Means (Version R Package Version 1.10.5)." https://cran.r-project.org/package=emmeans.

Leslie, M. S., L. Kant, C. Perkins-Taylor, et al. 2022. "Remote and Non-Invasive Quantification of 'Tattoo Skin Disease-Like' Dermatopathy in Endangered Arabian Sea Humpback Whales Using Drone Photography." *Mammalian Biology* 102, no. 4: 1605–1617.

Lo, C. F., H. H. Nollens, B. A. Nollens, et al. 2024. "Behavioral Responses of Bigg's and Southern Resident Killer Whales (*Orcinus orca*) to Uncrewed Aerial Vehicle-Based Breath Sample Collection."

Lonati, G. L., D. P. Zitterbart, C. A. Miller, P. Corkeron, C. T. Murphy, and M. J. Moore. 2022. "Investigating the Thermal Physiology of Critically Endangered North Atlantic Right Whales *Eubalaena glacialis* via Aerial Infrared Thermography." *Endangered Species Research* 48: 139–154.

Matthews, C. J. D., M. Ghazal, K. J. Lefort, and E. Inuarak. 2020. "Epizoic Barnacles on Arctic Killer Whales Indicate Residency in Warm Waters." *Marine Mammal Science* 36, no. 3: 1010–1014. https://doi.org/10.1111/mms.12674.

Mayaud, R., J. Castrillon, C. Wilson, et al. 2022. "Traffic in a Nursery: Ship Strike Risk From Commercial Vessels to Migrating Humpback Whales (*Megaptera novaeangliae*) in a Rapidly Developing Australian Urban Embayment." *Marine Policy* 146: 105332.

McGovern, B., A. F. Machernis, J. A. McCordic, et al. 2025. "Prevalence, Composition, and Behaviour of Humpback Whale (*Megaptera novaeangliae*) Groups Containing Multiple Mother-Calf Pairs in East Australia." *Aquatic Mammals* 51, no. 2: 163–177.

Mikhalev, Y. A. 1997. "Humpback Whales *Megaptera novaeangliae* in the Arabian Sea." *Marine Ecology Progress Series* 149: 13–21.

Millar, J., and G. Hickling. 1990. "Fasting Endurance and the Evolution of Mammalian Body Size." *Functional Ecology* 4: 5–12.

Minton, G., M. F. Van Bressem, A. Willson, et al. 2022. "Visual Health Assessment and Evaluation of Anthropogenic Threats to Arabian Sea Humpback Whales in Oman." *Journal of Cetacean Research and Management* 23, no. 1: 59–79. https://doi.org/10.47536/jcrm.v23i1.336.

Moore, M. J., T. K. Rowles, D. A. Fauquier, et al. 2021. "Assessing North Atlantic Right Whale Health: Threats, and Development of Tools Critical for Conservation of the Species." *Diseases of Aquatic Organisms* 143: 205–226.

Moreno-Colom, P., S. Ten, J. A. Raga, and F. J. Aznar. 2020. "Spatial Distribution and Aggregation of *Xenobalanus globicipitis* on the Flukes of Striped Dolphins, *Stenella coeruleoalba*: An Indicator of Host Hydrodynamics?" *Marine Mammal Science* 36, no. 3: 897–914.

Mount, R. 2005. "Acquisition of Through-Water Aerial Survey Images." *Photogrammetric Engineering & Remote Sensing* 71, no. 12: 1407–1415.

Muslim, A. M., W. S. Chong, C. D. M. Safuan, I. Khalil, and M. S. Hossain. 2019. "Coral Reef Mapping of UAV: A Comparison of Sun Glint Correction Methods." *Remote Sensing* 11, no. 20: 2422.

Napoli, C., N. Hirtle, J. Stepanuk, et al. 2024. "Drone-Based Photogrammetry Reveals Differences in Humpback Whale Body Condition and Mass Across North Atlantic Foraging Grounds." *Frontiers in Marine Science* 11: 1336455.

Newman, W. A., and D. P. Abbott. 1980. "Cirripedia: The Barnacles." *Intertidal Invertebrates of California* 504: 535.

Noad, M. J., E. Kniest, and R. A. Dunlop. 2019. "Boom to Bust? Implications for the Continued Rapid Growth of the Eastern Australian Humpback Whale Population Despite Recovery." *Population Ecology* 61, no. 2: 198–209.

O'Callaghan, S. A., F. Al Abbar, H. Costa, R. Prieto, M. Gammell, and J. O'Brien. 2024. "Aerial Photo-Identification of Sperm Whales (*Physeter macrocephalus*)." *Aquatic Mammals* 50, no. 6: 479–494.

Ólafsdóttir, D., and A. P. Shinn. 2013. "Epibiotic Macrofauna on Common Minke Whales, *Balaenoptera acutorostrata* Lacépède, 1804, in Icelandic Waters." *Parasites & Vectors* 6, no. 1: 105. https://doi.org/10.1186/1756-3305-6-105.

O'Mahony, É. N., A. L. Sremba, E. M. Keen, et al. 2024. "Collecting Baleen Whale Blow Samples by Drone: A Minimally Intrusive Tool for Conservation Genetics." *Molecular Ecology Resources* 24, no. 8: e13957. https://doi.org/10.1111/1755-0998.13957.

Omura, H. 1950. "Diatom Infection on Blue and Fin Whales in the Autarctic Whaling Area V-The Ross Sea Area." *Scientific Reports of the Whales Research Institute* 4: 14–26.

Osmond, M., and G. Kaufman. 1998. "A Heavily Parasitised Humpback Whale (*Megaptera novaeangliae*)."

Pallin, L. J., N. M. Kellar, D. Steel, et al. 2023. "A Surplus no More? Variation in Krill Availability Impacts Reproductive Rates of Antarctic Baleen Whales." *Global Change Biology* 29, no. 8: 2108–2121.

Peig, J., and A. J. Green. 2010. "The Paradigm of Body Condition: A Critical Reappraisal of Current Methods Based on Mass and Length." *Functional Ecology* 24, no. 6: 1323–1332. https://doi.org/10.1111/j.1365-2435.2010.01751.x.

Pettis, H. M., R. M. Rolland, P. K. Hamilton, S. Brault, A. R. Knowlton, and S. D. Kraus. 2004. "Visual Health Assessment of North Atlantic Right Whales (*Eubalaena glacialis*) Using Photographs." *Canadian Journal of Zoology* 82, no. 1: 8–19.

Pirotta, V., K. Owen, D. Donnelly, M. J. Brasier, and R. Harcourt. 2021. "First Evidence of Bubble-Net Feeding and the Formation of 'Super-Groups' by the East Australian Population of Humpback Whales During Their Southward Migration." *Aquatic Conservation: Marine and Freshwater Ecosystems* 31, no. 9: 2412–2419.

Pirotta, V., A. Smith, M. Ostrowski, et al. 2017. "An Economical Custom-Built Drone for Assessing Whale Health." *Frontiers in Marine Science* 4: 425.

Qiao, Y., X. Ma, B. Chen, S. Zhong, and X. Chen. 2020. "First Report of *Cyamus boopis* From A Humpback Whale (*Megaptera novaeangliae*) in the Coastal East China Sea."

R Core Team. 2024. *R: A Language and Environment for Statistical Computing*. R Foundation for Statistical Computing. https://www.r-project.org/.

Ramos, E. A., S. Landeo-Yauri, N. Castelblanco-Martínez, M. R. Arreola, A. H. Quade, and G. Rieucau. 2022. "Drone-Based Photogrammetry Assessments of Body Size and Body Condition of Antillean Manatees." *Mammalian Biology* 102, no. 3: 765–779.

Ramp, C., D. Gaspard, K. Gavrilchuk, et al. 2021. "Up in the Air: Drone Images Reveal Underestimation of Entanglement Rates in Large Rorqual Whales." *Endangered Species Research* 44: 33–44.

Raoult, V., A. P. Colefax, B. M. Allan, et al. 2020. "Operational Protocols for the Use of Drones in Marine Animal Research." *Drones* 4, no. 4: 64.

Ribbe, J. 2014. "Hervey Bay and Its Estuaries." In *Estuaries of Australia in 2050 and Beyond*, 185–201. Springer.

Robinson, C. V., and B. C. Visona-Kelly. 2025. "A Geometric Morphometric Approach for Detecting Different Reproductive Stages of a Free-Ranging Killer Whale *Orcinus orca* Population." *Scientific Reports* 15, no. 1: 3239. https://doi.org/10.1038/s41598-025-86793-3.

Rossi-Santos, M. R. 2015. "Oil Industry and Noise Pollution in the Humpback Whale (*Megaptera novaeangliae*) Soundscape Ecology of the Southwestern Atlantic Breeding Ground." *Journal of Coastal Research* 31, no. 1: 184–195.

Rother, C., V. Kolmogorov, and A. Blake. 2004. "'GrabCut' Interactive Foreground Extraction Using Iterated Graph Cuts." *ACM Transactions on Graphics (TOG)* 23, no. 3: 309–314.

Russell, G., A. Colefax, F. Christiansen, G. Russell, Z. Fowler, and D. Cagnazzi. 2022. "Body Condition and Migration Timing of East Australian Humpback Whales." *Marine Ecology Progress Series* 692: 169–183.

Ryan, K. P., S. H. Ferguson, W. R. Koski, B. G. Young, J. D. Roth, and C. A. Watt. 2022. "Use of Drones for the Creation and Development of a Photographic Identification Catalogue for an Endangered Whale Population." *Arctic Science* 8, no. 4: 1191–1201.

Segre, P. S. 2025. "A Practical Guide for Improving Confidence in Data Collected With Consumer-Level Drones." *Marine Mammal Science* 41: e70022.

Sekine, W., J. Kawasaki, K. Ohira, et al. 2025. "First Detection of an Alphaherpesvirus Gene in Humpback Whale Blow Samples Collected Noninvasively Using Unmanned Aerial Vehicles." *Viruses* 17, no. 11: 1411.

Sekrecka, A., D. Wierzbicki, and M. Kedzierski. 2020. "Influence of the Sun Position and Platform Orientation on the Quality of Imagery Obtained From Unmanned Aerial Vehicles." *Remote Sensing* 12, no. 6: 1040.

Serres, A., W. Lin, B. Liu, S. Chen, and S. Li. 2024. "Skinny Dolphins: Can Poor Body Condition Explain Population Decline in Indo-Pacific Humpback Dolphins (*Sousa chinensis*)?" *Science of the Total Environment* 917: 170401.

Shea, B. D., and A. J. Gallagher. 2021. "Humpback Whale Instigates Object Play With a Lion's Mane Jellyfish." *Oceans* 2, no. 2: 386–392.

Smith, C. E., S. T. Sykora-Bodie, B. Bloodworth, S. M. Pack, T. R. Spradlin, and N. R. LeBoeuf. 2016. "Assessment of Known Impacts of Unmanned Aerial Systems (UAS) on Marine Mammals: Data Gaps and Recommendations for Researchers in the United States." *Journal of Unmanned Vehicle Systems* 4, no. 1: 31–44.

Smith, J. N., H. S. Grantham, N. Gales, et al. 2012. "Identification of Humpback Whale Breeding and Calving Habitat in the Great Barrier Reef." *Marine Ecology Progress Series* 447: 259–272.

Soledade Lemos, L., J. D. Burnett, T. E. Chandler, J. L. Sumich, and L. G. Torres. 2020. "Intra- and Inter-Annual Variation in Gray Whale Body Condition on a Foraging Ground." *Ecosphere* 11, no. 4: e03094. https://doi.org/10.1002/ecs2.3094.

Sorrell, K. J., R. H. Clarke, R. Holmberg, and R. R. McIntosh. 2019. "Remotely Piloted Aircraft Improve Precision of Capture–Mark–Resight

Population Estimates of Australian Fur Seals." *Ecosphere* 10, no. 8: e02812.

Sprogis, K. R., and F. Christiansen. 2024. "Allosuckling in Southern Right Whale Calves." *Mammalian Biology* 104, no. 1: 91–99.

Sprogis, K. R., D. Holman, P. Arranz, and F. Christiansen. 2023. "Effects of Whale-Watching Activities on Southern Right Whales in Encounter Bay, South Australia." *Marine Policy* 150: 105525.

Stack, S., J. Currie, J. McCordic, A. Machernis, and G. Olson. 2019. "Distribution Patterns of East Australian Humpback Whales (*Megaptera novaeangliae*) in Hervey Bay, Queensland: A Historical Perspective." *Australian Mammalogy* 42, no. 1: 16–27.

Stack, S. H., L. Krannichfeld, and B. Romano. 2024. "An Observation of Sexual Behavior Between Two Male Humpback Whales." *Marine Mammal Science* 40: e13119.

Stack, S. H., K. R. Sprogis, G. L. Olson, F. A. Sullivan, A. F. Machernis, and J. J. Currie. 2021. "The Behavioural Impacts of Commercial Swimming With Whale Tours on Humpback Whales (*Megaptera novaeangliae*) in Hervey Bay, Australia." *Frontiers in Marine Science* 8: 696136.

Stamation, K. A., D. B. Croft, P. D. Shaughnessy, and K. A. Waples. 2007. "Observations of Humpback Whales (*Megaptera novaeangliae*) Feeding During Their Southward Migration Along the Coast of Southeastern New South Wales, Australia: Identification of a Possible Supplemental Feeding Ground." *Aquatic Mammals* 33, no. 2: 165.

Sykora-Bodie, S. T., V. Bezy, D. W. Johnston, E. Newton, and K. J. Lohmann. 2017. "Quantifying Nearshore Sea Turtle Densities: Applications of Unmanned Aerial Systems for Population Assessments." *Scientific Reports* 7, no. 1: 17690.

Taylor, L. D., A. O'Dea, T. J. Bralower, and S. Finnegan. 2019. "Isotopes From Fossil Coronulid Barnacle Shells Record Evidence of Migration in Multiple Pleistocene Whale Populations." *Proceedings of the National Academy of Sciences of the United States of America* 116, no. 15: 7377–7381.

Ten, S., G. Dupont, J. A. Raga, A. P. Dobson, and F. J. Aznar. 2026. "Long-Term Trends of Epibionts Reflect Mediterranean Striped Dolphin Abundance Shifts Caused by Morbillivirus Epidemics." *Journal of Animal Ecology* 95: 553–569.

Ten, S., F. Fusar Poli, K. Konishi, et al. 2025. "The Epibiont *Xenobalanus globicipitis* Indicates Differences in Swimming Kinematics Among Cetaceans." *Marine Biology* 172, no. 1: 1–15.

Ten, S., K. Konishi, J. A. Raga, L. A. Pastene, and F. J. Aznar. 2022. "Epibiotic Fauna of the Antarctic Minke Whale as a Reliable Indicator of Seasonal Movements." *Scientific Reports* 12, no. 1: 22214. https://doi.org/10.1038/s41598-022-25929-1.

Ten, S., J. Raga, and F. Aznar. 2022. "Epibiotic Fauna on Cetaceans Worldwide: A Systematic Review of Records and Indicator Potential." *Frontiers in Marine Science* 9: 846558.

Thomas, P. O., R. R. Reeves, and R. L. Brownell Jr. 2016. "Status of the World's Baleen Whales." *Marine Mammal Science* 32, no. 2: 682–734.

Toms, C. N., T. Stone, and T. Och-Adams. 2020. "Visual-Only Assessments of Skin Lesions on Free-Ranging Common Bottlenose Dolphins (*Tursiops truncatus*): Reliability and Utility of Quantitative Tools." *Marine Mammal Science* 36, no. 3: 744–773.

Torres, L. G., S. L. Nieukirk, L. Lemos, and T. E. Chandler. 2018. "Drone Up! Quantifying Whale Behavior From a New Perspective Improves Observational Capacity." *Frontiers in Marine Science* 5: 319.

Torres, W. I., and K. Bierlich. 2020. "MorphoMetriX: A Photogrammetric Measurement GUI for Morphometric Analysis of Megafauna." *Journal of Open Source Software* 5, no. 45: 1825.

Towers, J. R., C. J. McMillan, M. Malleson, J. Hildering, J. K. Ford, and G. M. Ellis. 2013. "Seasonal Movements and Ecological Markers as Evidence for Migration of Common Minke Whales Photo-Identified in the Eastern North Pacific." *Journal of Cetacean Research and Management* 13, no. 3: 221–229.

Urian, K., A. Gorgone, A. Read, et al. 2015. "Recommendations for Photo-Identification Methods Used in Capture-Recapture Models With Cetaceans." *Marine Mammal Science* 31, no. 1: 298–321.

Urian, K. W., R. Kaufmann, D. M. Waples, and A. J. Read. 2019. "The Prevalence of Ectoparasitic Barnacles Discriminates Stocks of Atlantic Common Bottlenose Dolphins (*Tursiops truncatus*) at Risk of Entanglement in Coastal Gill Net Fisheries." *Marine Mammal Science* 35, no. 1: 290–299. https://doi.org/10.1111/mms.12522.

Vargas-Castro, I., J. L. Crespo-Picazo, M. Á. Jiménez Martínez, et al. 2024. "Molecular Detection of Herpesvirus in a Skin Lesion of a Humpback Whale (*Megaptera novaeangliae*) From the Western Mediterranean Sea." *European Journal of Wildlife Research* 70, no. 2: 31. https://doi.org/10.1007/s10344-024-01782-7.

Vilches, F. O., M. Sironi, A. N. Zerbini, S. J. Fernández, M. M. Uhart, and V. J. Rowntree. 2023. "Life Histories of Satellite-Tracked Southern Right Whales Through Photo-Identification and Citizen Science in Patagonia, Argentina." *Aquatic Mammals* 49, no. 2: 167–176.

Visser, I. N., T. E. Cooper, and H. Grimm. 2020. "Duration of Pseudo-Stalked Barnacles (*Xenobalanus globicipitis*) on a New Zealand Pelagic Ecotype Orca (*Orcinus orca*), With Comments on Cookie Cutter Shark Bite Marks (*Isistius* sp.); Can They Be Used as Biological Tags." *Biodivers Journal* 11: 1067–1086.

Vivier, F., R. S. Wells, M. C. Hill, et al. 2023. "Quantifying the Age Structure of Free-Ranging Delphinid Populations: Testing the Accuracy of Unoccupied Aerial System Photogrammetry." *Ecology and Evolution* 13, no. 6: e10082.

von Hammerstein, H., R. O. Setter, M. van Aswegen, J. J. Currie, and S. H. Stack. 2022. "High-Resolution Projections of Global Sea Surface Temperatures Reveal Critical Warming in Humpback Whale Breeding Grounds." *Frontiers in Marine Science* 9: 837772.

Warton, D. I., R. A. Duursma, D. S. Falster, and S. Taskinen. 2012. "Smatr 3—An R Package for Estimation and Inference About Allometric Lines." *Methods in Ecology and Evolution* 3, no. 2: 257–259. https://doi.org/10.1111/j.2041-210X.2011.00153.x.

Whitehead, T. O., D. P. Rollinson, and R. R. Reisinger. 2015. "Pseudostalked Barnacles *Xenobalanus globicipitis* Attached to Killer Whales *Orcinus orca* in South African Waters." *Marine Biodiversity* 45, no. 4: 873–876. https://doi.org/10.1007/s12526-014-0296-2.

Wikelski, M., and S. J. Cooke. 2006. "Conservation Physiology." *Trends in Ecology & Evolution* 21, no. 1: 38–46.

Wirsing, A. J., A. N. Johnston, and J. J. Kiszka. 2022. "Foreword to the Special Issue on 'the Rapidly Expanding Role of Drones as a Tool for Wildlife Research'." *Wildlife Research* 49, no. 1: 1–5.

Supporting Information

Additional supporting information can be found online in the Supporting Information section. **Table S1:** mms70255-sup-0001-Table_S1-S5-Figure_S1-S5.docx. **Table S1:1:** Mean and standard deviation (SD) of barnacle epibiont-affected percentage coverage estimated from imagery of standardized dorsal-surface anatomies obtained from vessel- and drone-based sampling platforms, and the corresponding difference in percentage coverage between imaging platforms. Values were calculated using six randomly selected paired image sets ($n = 6$), with each paired image, identified by Sample ID, measured five times to assess variance in segmentation techniques, including manual marking. Vessel-based image quality was scored on a five-point scale: 5 (*excellent*), 4 (*good*), 3 (*average*), 2 (*fair*), and 1 (*poor*). **Table S1:2:** Model-selection results for generalized linear mixed-effects models (GLMMs), ranked by corrected Akaike Information Criterion (AICc). Two model families were constructed: (1) beta regression GLMMs with a logit link to evaluate proportional epibiont coverage estimates, and (2) Gaussian distribution GLMMs with an identity link to assess log-transformed binary image mask (BIM) pixel counts. Predictors included categorical variables: sampling platform technique (drone- vs. vessel-based method; 2 levels), BIM type (4 levels), epibiont characteristic (2 levels), anatomical region sampled (3 levels), and age class (3 levels), along with the continuous covariates time of day (h) and ground sampling distance (GSD). Beta regression models included interactions between sampling technique and all other predictors, while top-supported Gaussian distribution models did not. A random intercept for Sample ID was included in all models. Final model support is indicated by delta AICc (ΔAICc). **Table S1:3:** Summary of final GLMM with a beta regression distribution for proportional epibiont coverage as a function of the main effects: sampling method (drone vs. vessel image data) and epibiont characteristic (barnacle scarring vs. attached), including the interaction term: time of day (h) and sampling method. The estimated coefficients (β) represent the logit scale of the expected proportion. The model consists of a random intercept for Sample ID. The universal precision ($ø$) parameter was not modeled. **Table S1:4:** Summary of the final Gaussian GLMM for log-transformed pixel values from masked imagery using paired vessel- and drone-based samples. Fixed effects included age class, binary image mask (BIM) measurement type, and time of day (h) at paired image capture; Sample ID was included as a random intercept. Coefficients (β) are reported as contrasts relative to the reference levels (DBIM1 for mask type; Calf for age class). Reported estimates are on the log-transformed scale for interpretability. **Table S1:5:** Pairwise contrasts of estimated marginal means (EMMs) from the Gaussian GLMM (identity link) for log-transformed pixel counts derived from binary image masks (BIMs). Tukey-adjusted pairwise comparisons are shown for BIM measurement type (DBIM1, DBIM2, VBIM1, VBIM2) and age class (calves, subadults, adults). All contrasts are averaged over the levels of the non-focal predictor. **Figure S1:** Exemplary drone video stills used for quantifying epibiont coverage that (a) met the robust selection criteria (ROS22_0323) and (b) were excluded from pixel-based analysis (DSF22_5365). **Figure S2:** Color-channel isolation for working within the CIELAB color space is also referred to as $L^*a^*b^*$, using a vessel-based image (ROS22_0851): (a) original input image, (b) L^* channel: luminance or perceptual lightness, (c) a^* channel: high red-low green, and (d) b^* channel: high yellow-low blue. **Figure S3:** Pixel-based analysis of proportional barnacle epibiont coverage (%) for 32 paired image samples from Breeding Stock E1 humpback whales photographed during concurrent drone- and vessel-based surveys in Hervey Bay, Queensland, and Eden, New South Wales, in 2022 and 2023. Purple points denote raw estimates from drone video stills, and yellow points denote raw estimates from vessel-based images. Sample IDs indicate the standardized dorsal-surface anatomical regions used for pairwise comparison: dorsal-side flukes (DSF), pectoral fin (PEC), and rostral area (ROS). Error bars represent the standard deviation (SD) of coverage estimates for six randomly selected paired samples measured multiple times. **Figure S4:** Pixel-based quantification of the proportional coverage of colonized juvenile coronulids on a post-neonate humpback whale calf photographed by drone in Hervey Bay in 2022, for which no vessel-based image was available for quantitative comparison. Panels (a) and (d) show the original input images of the rostrum and dorsal surface of the flukes, respectively. Panels (b) and (e) show the secondary epibiont binary image masks created through color thresholding of the segmented anatomy masks. Panels (c) and (f) show the original images overlaid with the segmented areas affected by colonized epibionts (magenta), estimated at 29.62% and 13.26% proportional coverage, respectively. **Figure S5:** Pixel-based quantification of the proportional coverage of colonized juvenile coronulids on the rostrum of a post-neonate humpback whale calf photographed by drone in Hervey Bay in 2022, for which no vessel-based image was available for quantitative comparison. (a) Original input image. (b) Segmented area affected by epibionts following color thresholding. (c) Original input image overlaid with the segmented mask (magenta). Proportional coverage of the visible rostral area is estimated at 18.27%.